NUMERICAL ANALYSIS OF TURBULENT BOUNDARY LAYERS ON ROUGH WALLS USING A NEAR-WALL RANS MODEL

A Thesis submitted to the College of

Graduate and Postdoctoral Studies

In Partial Fulfillment of the Requirements

For the Degree of Master of Science

In the Department of Mechanical Engineering

University of Saskatchewan

Saskatoon

By

Minghan Chu

PERMISSION TO USE

The author grants permission to the University of Saskatchewan Libraries to make this thesis available for inspection. Copying of this thesis, in whole or in part, for scholarly purposes may be granted by my supervisor, Prof. D. J. Bergstrom, or the Department Head of the college of Engineering. It is understood that any copying or publication or use of this thesis or part thereof for financial gain shall not be allowed without my written permission. It is also understood that due recognition to me and the University of Saskatchewan must be granted in any scholarly use which may be made of any material in this thesis.

Request for permission to copy or to make other use of material in this thesis in whole or in part should be addressed to:

Head of the Department of Mechanical Engineering

57 Campus Drive

University of Saskatchewan

Saskatoon, Saskatchewan S7N 5A9

Canada

OR

Dean

College of Graduate and Postdoctoral Studies

University of Saskatchewan

116 Thorvaldson Building, 110 Science Place

Saskatoon, Saskatchewan S7N 5C9

Canada

ABSTRACT

Near-wall turbulent flows are frequently encountered in environmental and engineering applications. Surface roughness is often present, frequently with an inhomogeneous distribution. One classical example of such a flow is the internal boundary layer (IBL) formed downstream of a step change from a smooth to a rough surface on a flat plate. Computational fluid dynamics modeling of turbulent flow over rough surfaces remains a significant challenge, especially for more complex roughness configurations.

In this thesis, a numerical study was carried out to assess the ability of the Reynolds-Averaged Navier-Stokes, or RANS-based two-layer $k-\varepsilon$ model developed by Durbin *et al.* (2001) to predict two different rough-wall flows. The two-layer model introduces a hydrodynamic roughness length, y_0, to implement the effects of roughness. Firstly, fully developed turbulent flow in a vertical pipe was simulated to benchmark the model, and investigate the predictions of the mean velocity and turbulence fields in the region very close to the wall. The second simulation considered the IBL created by an abrupt transition from a smooth to a rough surface on a flat plate, with the focus of the study being the effects of roughness on the mean velocity and turbulence fields as they develop downstream of the step.

For the turbulent pipe flow, the model correctly predicted the downward shift of the mean velocity profiles for both the transitionally-rough and fully-rough flow cases compared to that of the smooth flow case. The value of the eddy viscosity for the fully-rough flow was finite at the wall and close to the value of the molecular viscosity. The profiles of Reynolds shear stress and turbulence kinetic energy for the fully-rough flow both exhibited two peaks in the near-wall region, with one located at the wall. The turbulence kinetic energy budget for the fully rough flow exhibited a peak value in the dissipation at the wall that was much larger than the production. As such, in the model formulation the roughness dramatically changed the mean velocity and turbulence properties at the wall.

For case of the IBL flow, a transition and equilibrium zone were predicted downstream of the step. In the transition zone, the mean velocity profile in the lower region exhibited the effects of surface roughness, whereas the mean velocity profile further away from the plate retained the

characteristics of the smooth wall boundary layer upstream of the step. For the equilibrium zone, the flow was in equilibrium with the rough surface throughout the entire boundary layer. A novel method was used to determine the thickness of the IBL based on the turbulence kinetic energy profile in the transition zone. The model predicted a growth rate for the IBL that agreed well with other studies in the literature. For the transition zone, both the Reynolds shear stress and turbulence kinetic energy profiles showed a collapse and recovery cycle. Just as for the pipe flow, the roughness significantly modified the Reynolds shear stress and turbulence kinetic energy very close to the roughness elements.

ACKNOWLEDGEMENTS

I would like to express my earnest gratitude and my profound appreciation to my respected supervisor, Prof. D. J. Bergstrom. Thank you so much for your invaluable guidance, support and inspiration throughout my work during my graduate program. I have made much progress on better writing, confident presenting, and deep thinking during my graduate program because of you.

I would also like to express a very big appreciation to my friend Wei Cheng Qian who is a PhD student majoring in computer science at the University of Saskatchewan. During my graduate program, he spent much time helping me solve the Fortran problems I came up with. With his help, I not only solved the problems, but I also gained insight into coding and learned how and why I could be more effective when programming and debugging.

I take this opportunity to thank my research colleagues of the CFD group for their assistance and my intimate friends at Department of Computer Science for giving me a lot insights into their realms of study.

My thanks also goes to my father, Mr. Chengling Chu, and my mother, Mrs. Chunqiu Zheng. Your solid trust, encouragement and support are greatly appreciated.

DEDICATION

This thesis is dedicated to my parents, Chenglin Chu and Chunqiu Zheng for their generous support and motivation.

TABLE OF CONTENTS

PERMISSION TO USE ..... **i**
ABSTRACT ..... **ii**
ACKNOWLEDGEMENTS ..... **iv**
DEDICATION ..... **v**
TABLE OF CONTENTS ..... **vi**
LIST OF FIGURES ..... **ix**
LIST OF TABLES ..... **xi**
LIST OF SYMBOLS ..... **xii**

CHAPTER ONE: INTRODUCTION **1**
1.1 Background 1
1.2 Turbulent boundary layer and surface roughness 1
1.21 Surface roughness effects 2
1.3 Internal boundary layer 3
1.4 Motivation for considering the internal boundary layer 3
1.5 Objectives and scope 4
1.6 Methodology 5
1.61 RANS turbulence model 5
1.62 Numerical method 7
1.7 Thesis organization 8
1.8 References 9

CHAPTER TWO: PREDICTION OF TURBULENT FLOW IN A ROUGH PIPE USING A NEAR-WALL RANS MODEL 11

Abstract 12

2.1 Introduction 13

2.2 The two-layer $k - \varepsilon$ model 14

2.2.1 Governing equations 14

2.2.2 The effect of roughness 17

2.3 Flow description and numerical method 19

2.4 Results and discussion 20

2.4.1 Mean velocity profile 20

2.4.2 Roughness shift 21

2.4.3 Mean velocity gradient 21

2.4.4 Eddy viscosity 22

2.4.5 Reynolds shear stress 23

2.4.6 Turbulence kinetic energy 24

2.4.7 Energy budget 24

2.4.8 Darcy friction factor 26

2.5 Conclusions 26

2.6 References 28

CHAPTER THREE: PREDICTION OF TURBULENT FLOW OVER A FLAT PLATE WITH A STEP CHANGE FROM A SMOOTH TO A ROUGH SURFACE USING A NEAR-WALL RANS MODEL 38

Abstract 39

3.1 Introduction 40

3.2 The two-layer $k-\varepsilon$ model 43
3.2.1 Incorporating the effect of roughness 43
3.2.2 Governing equations 44
3.2.3 Flow description and numerical method 48
3.3 Results and discussion 50
3.3.1 Skin friction coefficient 50
3.3.2 Evaluating the height of the IBL 51
3.3.3 Streamwise mean velocity 52
3.3.4 Mean streamwise velocity using inner coordinates 53
3.3.5 Mean defect velocity profile 54
3.3.6 Reynolds shear stress profiles 55
3.3.7 Turbulence kinetic energy profile 56
3.4 Conclusions 57
3.5 References 59

CHAPTER FOUR: CONCLUDING REMARKS AND FUTURE WORK 71

4.1 Summary and conclusion 71
4.1.1 Rough wall pipe flow 71
4.1.2 IBL created by smooth-rough transition 72
4.2 Future work 73

APPENDIX 75

The standard $k-\varepsilon$ model 75
Standard wall functions 76

LIST OF FIGURES

Figure 2.1: Schematic of y_{eff} and y_o relative to the roughness elements **31**

Figure 2.2: Schematic of the flow geometry **31**

Figure 2.3: Mean velocity profiles using inner coordinates **32**

Figure 2.4: Roughness shift as a function of equivalent sand-grain roughness **32**

Figure 2.5: The profile of normalized mean velocity gradient **33**

Figure 2.6: a) The profile of normalized eddy viscosity; b) expanded version in the region very close to the wall **34**

Figure 2.7: The profile of normalized Reynolds shear stress on: a) linear scale; b) logarithmic scale **35**

Figure 2.8: The profile of normalized turbulence kinetic energy on: a) linear scale; b) logarithmic scale **36**

Figure 2.9: The profile of normalized production and viscous dissipation **37**

Figure 3.1: Schematic of y_{eff} and y_o relative to the roughness elements **62**

Figure 3.2: Schematic of the flow geometry **62**

Figure 3.3: Prediction for skin friction coefficient distribution over the plate **63**

Figure 3.4: Defining the IBL thickness based on profile for the turbulence kinetic energy **63**

Figure 3.5: Defining the IBL thickness using the inflection point method of Antonia and Luxton (1971).....**64**

Figure 3.6: Streamwise growth of the IBL: δ_i based on the turbulence kinetic energy, and δ_{ip} based on the inflection point method of Antonia and Luxton (1971).....**64**

Figure 3.7: Streamwise growth of the IBL thickness compared to the outer BL thickness **65**

Figure 3.8: a) Streamwise mean velocity profiles in the transition zone; b) Streamwise mean velocity profiles in the equilibrium zone **66**

Figure 3.9: a) Profile of normalized mean velocity for wall-normal direction; b) enlarged version of a) for $y_{eff}^{+} > 100$ **67**

Figure 3.10: Mean velocity defect velocity profile normalized by u_{τ} **68**

Figure 3.11: a) Profile of normalized Reynolds shear stress; b) replotted using logarithmic scale for wall-normal distance **69**

Figure 3.12: a) Profile of normalized turbulence kinetic energy; b) replotted using logarithmic scale for wall-normal distance **70**

LIST OF TABLES

Table 2.1: ν_t/ν at the first grid node 30

Table 2.2: Comparison of Darcy friction factor.....30

LIST OF SYMBOLS

A_v^0	two-layer model constant
A_ε	two-layer model constant
A_v	two-layer model constant
$C_{\varepsilon 1}$	two-layer model constant
C_l	two-layer model constant
$C_{\varepsilon 2}$	two-layer model constant
C_v	two-layer model constant
c_f	skin friction coefficient
D_k	diffusion term for turbulence kinetic energy
D_ε	diffusion term for turbulence dissipation
f	Darcy friction factor
g_x	gravitational acceleration in x direction
g_y	gravitational acceleration in y direction
k	turbulence kinetic energy
k_{sg}	sand-grain roughness height
l	turbulent length scale
L	flat-plate length
P	streamwise mean pressure
P_k	production term for turbulence kinetic energy
r	radial coordinate

R	pipe radius
Re_d	bulk Reynolds number
Re_θ	Reynolds number based on momentum thickness
R_y	Reynolds number based on wall-normal distance
u_τ	friction velocity
U_z	streamwise mean velocity for pipe flow
u_r	radial fluctuation velocity for pipe flow
u_z	streamwise fluctuation velocity for pipe flow
U	streamwise mean velocity for flat plate flow
U_r	radial mean velocity for pipe flow
V	wall-normal mean velocity for flat plate flow
x	streamwise direction for flat plate flow
x'	distance after step on rough surface
x_s	the station ahead of the step on the smooth surface
x_1 to x_9	the stations after the step on the rough surface
y	wall-normal distance
y_{eff}	effective wall-normal distance
y_0	hydrodynamic roughness
z	streamwise coordinate for pipe flow
$< u_z u_r >$	Reynolds shear stress for pipe flow
$< u^2 >$	Reynolds normal stress for flat plate flow
$< v^2 >$	Reynolds normal stress for flat plate flow

$< uv >$	Reynolds shear stress for flat plate flow

Greek symbols

δ	outer boundary thickness
δ_i	thickness of internal boundary layer determined using turbulence kinetic energy
δ_{ip}	thickness of internal boundary layer determined using the method of Antonia and Luxton (1971)
ε	turbulence dissipation
κ	von Karman's constant
ν	kinematic viscosity
ρ	density
σ_k	two-layer model constant
σ_ε	two-layer model constant

Mathematical symbols

< >	time-averaging

Subscripts

d	pertaining to the pipe diameter
eff	pertaining to the concept of effective wall-normal distance
f	pertaining to the friction on turbulent flow
i	pertaining to the method from turbulence kinetic energy
ip	pertaining to the method from Antonia and Luxton (1971)
k	pertaining to the turbulence kinetic energy
l	pertaining to the turbulent length scale
r	pertaining to the radial direction
s	pertaining to the smooth surface
t	pertaining to turbulent flow
x	pertaining to the x component in the Cartesian coordinate
y	pertaining to the y component in the Cartesian coordinate
z	pertaining to the streamwise direction for pipe flow
$1-9$	pertaining to the positions for rough surface
τ	pertaining to shear stress
sg	pertaining to sand-grain roughness
ε	pertaining to dissipation
ν	pertaining to viscosity
θ	pertaining to momentum thickness
0	pertaining to the concept of hydrodynamic roughness length

Superscripts

$'$	pertaining to the distance after the step
$+$	pertaining to the normalized quantity of the flow

CHAPTER ONE

INTRODUCTION

1.1 Background

Turbulent flow is the flow regime most frequently encountered in engineering applications, such as oil pipelines and flow over aircraft. Often these flows are over walls, in which case surface roughness can be present, e.g. rust growing on the interior surface of a pipe or icing on an airfoil. Therefore, the accurate prediction of the effect of wall roughness on turbulent flow and heat transfer is of great interest for engineering applications. Numerical methods that have been developed to capture the important effects of turbulence can be categorized into Reynolds-Averaged Navier-Stokes (RANS) methods, large eddy simulation (LES), and direct numerical simulation (DNS). For computational predictions that use a RANS formulation, the turbulence model for the Reynolds stress needs to be modified in the near-wall region to account for the effect of wall roughness.

Turbulent flow over rough surfaces is challenging both to understand and to model. Recall that roughness breaks up the viscous sublayer and enhances the local wall shear stress. Presently turbulence models are not able to predict a skin friction distribution based on the surface geometry alone. Furthermore, most studies on modeling the hydrodynamic effects of surface roughness have focused on homogeneous distributions of roughness elements and studied the boundary layers that develop on them. However, in industrial and environmental applications, the surface roughness is often localised, which can lead to the formation of a so-called internal boundary (IBL). An IBL is frequently encountered in engineering and environmental applications, e.g., icing on the surface of an airfoil, rusting on the interior surface of a pipe, and wind passing from water to land. There is a need to better understand these flow scenarios.

1.2 Turbulent boundary layer and surface roughness

When a turbulent flow passes over a solid wall, a turbulent boundary layer is formed. Prandtl in 1904 deduced that boundary layer is thin when the Reynolds number is sufficiently large. For a smooth-wall flow scenario, a mean streamwise velocity profile is formed due to the no-slip

boundary condition at the wall. In the wall-normal direction the value of the mean streamwise velocity gradually increases and eventually reaches the freestream velocity value at the outer edge of the boundary layer. The boundary layer thickness is defined to be the location above the wall at which the local mean velocity reaches 99% of the freestream velocity.

1.2.1 Surface roughness effects

Roughness refers to protrusions and/or cavities on wall surfaces that can increase the frictional resistance in the flow. Turbulent flows are strongly affected by roughness. If roughness penetrates through the viscous sublayer next to the wall, the turbulent boundary layer is broken up, and the inner layer of the log-law is modified. Roughness can reduce the velocity in the near-wall region, and increase the local wall shear stress, which in turn results in a higher production of turbulence. Schlichting (1979) defined three regimes based on the effect of roughness on turbulent flow:

1. Hydraulically smooth ($k_{sg}^{+} < 5$): turbulent transport against the flow can be completely neglected compared to viscous transport in which the fluid retains the characteristics of unsteady laminar flows,
2. Transitionally rough ($5 \leq k_{sg}^{+} \leq 70$): both turbulent and viscous transports are significant,
3. Fully rough ($k_{sg}^{+} > 70$): viscous transport is negligibly small compared to turbulent friction.

In the above, the dimensionless sand-grain roughness is given by $k_{sg}^{+} = k_{sg} u_\tau / \nu$, and k_{sg} and u_τ are the sand-grain roughness length and friction velocity, respectively. The concept of sand-grain roughness is largely due to Nikuradse (1933), who performed experiments to obtain systematic and extensive measurements on rough circular pipes with sand grains glued onto the internal wall. In practice, many engineering applications have a much smaller roughness density than that considered by Nikuradse (1933) and special techniques are needed to compute their corresponding equivalent sand-grain roughness.

1.3 Internal boundary layer

When a turbulent flow passes over a step change in surface roughness the effects of the surface roughness on the flow downstream of the step is characterized by an IBL. The term 'internal' is adopted since the new boundary layer develops within the outer boundary layer upstream of the step. Antonia and Luxton (1971) performed an experimental study of the flow behavior after a smooth-to-rough step change in roughness for a zero pressure gradient boundary layer, with the level of the rough surface depressed below the smooth surface upstream of the step. They determined the IBL thickness using a half-power law method, where the outer edge of the IBL is defined by the location of a 'knee' point characterised by a distinct change in slope. Lee and Sung (2007, 2011) used a DNS to analyze the effect of different roughness geometry on the IBL formed downstream of smooth-to-rough transition. Rao (1973), from an environmental point of view, modeled a two-dimensional IBL based on the second moment turbulence model proposed by Lumley and Khajeh-Nouri (1974) which used transport equations for the Reynolds stresses and viscous dissipation rate. Savelyev and Taylor (2005) stated that an internal boundary layer comprises an equilibrium layer immediately above the surface, and a transition layer, within which an inflection point pertaining to the mean velocity profile can be observed. Pendergrass and Arya (1984) defined the equilibrium layer as the layer in which the flow is undergoing a rapid transition process from the equilibrium characteristics in the inner layer to that of the outer layer retaining the boundary conditions upstream of the step. Within the IBL created by the flow over an abrupt transition from a smooth to a rough surface, the region close to the surface experiences the change in roughness, and the effect of roughness propagates deeper into the outer boundary layer as the flow develops downstream of the step.

1.4 Motivation for considering the internal boundary layer

Roughness is not always homogenous in practice. Surfaces in the industry and environment are not always uniformly rough. IBLs frequently occur in environmental and diverse engineering and industrial applications, e.g. wind transitioning from water to land and erosion of turbine blades. The perturbations triggered by roughness can alter the structure of the boundary layer close to the wall, which in turn influences the momentum, heat, and mass transfer rates at the surface. Patel (1998) identified the challenge of modeling high Reynolds number flows over rough surfaces as a

significant challenge for computational fluid dynamics (CFD). Twenty years later, this assessment is still valid. The roughness associated with cavities in the surface of a solid wall, e.g. erosion, might have a slightly different effect on turbulent flow than roughness elements located above the surface of a solid wall, e.g. rust. Numerical and experimental studies addressing this issue are deficient. As indicated in the study of Krogstad and Antonia (1999), the wall geometry strongly affects the turbulent transport mechanisms, especially for the near-wall region. Turbulence models using the sand-grain roughness approach need to be modified to better predict the flows with more complex roughness encountered in many applications.

1.5 Objectives and scope

The overall objective of the research is to explore the capability of the RANS-based, two-layer, $k-\varepsilon$ model of Durbin *et al.* (2001) to predict the effect of roughness on the mean velocity and turbulence fields in a near-wall flow with significant streamwise development, i.e. an internal boundary layer. The study is further broken down into the two following specific objectives:

1. Use the two-layer turbulence model to predict the velocity field in fully developed (one-dimensional, 1D) pipe flow for three different roughness regimes, i.e. hydraulically smooth, transitionally rough and fully rough. This will allow the near-wall features predicted for the flow field to be explored in detail.
2. Use the two-layer model to predict a spatially developing (two-dimensional, 2D) IBL created by an abrupt transition from a smooth to a fully rough surface. This will test the ability of the model to predict a flow where the surface condition in terms of roughness is inhomogeneous.

The contributions of the present study include the following:

1. Document the performance of the two-layer $k-\varepsilon$ turbulence model in the near-wall region, especially the predictions for the mean and turbulence fields in the proximity of the rough surface. This information is typically missing in previous studies which use this model.
2. Assess the performance of the two-layer $k-\varepsilon$ turbulence model in modeling a flow where the roughness is inhomogeneous in the streamwise direction.

3. Compare the predictions for the IBL using a RANS turbulence model to the experimental results in the literature, and assess their validity.

The study will be accomplished using two different in-house Fortran codes (1D and 2D). The 1D Fortran code has been extensively studied by number of students for single phase and multiphase flows. The two-dimensional was originally developed by professor Donald Bergstrom. The motivation for using in-house code was to have complete transparency and control in terms of the implementation of the two-layer $k-\varepsilon$ turbulence model. Although both codes were pre-existing, they required significant work to re-configure for the present simulations. The 2D code in particular required substantial overhaul and reconfiguration for the IBL simulation, including an extensive exploration of the grid configuration and boundary conditions.

The IBL simulation did not aim to reproduce specific experiments, since no such experiments were available. However, general comparisons were made to the data generated by DNS and experimental studies.

1.6 Methodology

The present section briefly describes the methodology used in the current research, specifically the RANS approach, and the numerical method. Specific details of the two-layer model are given in the manuscripts documented in chapter 2 and 3.

1.6.1 RANS turbulence model

The Reynolds Averaged Navier-Stokes (RANS) equations solve for time-averaged properties of a turbulent flow. The RANS equations are obtained by decomposing the instantaneous flow property into its time-averaged and fluctuating quantities. Using this approach, which is referred to as Reynolds decomposition, the RANS equations can be derived from the Navier-Stokes equations. For steady, incompressible, turbulent flow of a Newtonian fluid with no thermal interactions, the differential Reynolds-averaged mass and momentum equations in Cartesian tensor notation can be written as follows:

$$\frac{\partial(\rho U_j)}{\partial x_j} = 0 \tag{1.1}$$

$$\rho U_j \frac{\partial U_i}{\partial x_j} = -\frac{\partial P}{\partial x_i} + \frac{\partial}{\partial x_j}\left(\mu \frac{\partial U_i}{\partial x_j} - \rho < u_i u_j >\right) + \rho g_i \tag{1.2}$$

where U_i and u_i are the ith component of the mean and fluctuating velocity field, respectively, P is the mean pressure field, x_j denotes the jth coordinate direction, ρ is the density, μ is the dynamic viscosity and g_i is the gravitational acceleration. The term $\rho < u_i u_j >$ has the same dimension as the Newtonian (laminar) stress term and is referred to as the Reynolds stress tensor, although it is a nonlinear convective term. The Reynolds stresses are unknown turbulence quantities that need to be accurately modelled to close the mean mass and momentum equations. The models used to estimate the Reynolds stresses in the RANS equations are often referred to simply as turbulence models, and can be classified into algebraic models, two-equation models, etc. The Reynolds stress model (RSM), or second moment closure model, is regarded as the most complex and realistic turbulence model among the RANS models. It solves the transport equations for the Reynolds stress tensor. However, for industrial applications, it is more common to use an eddy viscosity model for the constitutive relation, and couple it with a two-equation closure that uses two additional transport equations to calculate the turbulent or eddy viscosity. The most popular two-equation closure is the $k - \varepsilon$ model, which consists of transport equations for the turbulence kinetic energy k and its dissipation rate ε. The $k - \varepsilon$ model performs well in simple turbulent boundary layer flows, e.g. duct and boundary layer flows, in which Reynolds shear stresses can be related to the single mean velocity gradient. The standard $k - \varepsilon$ model equations are presented in Appendix A.

For a turbulent boundary layer flow, any RANS model needs to be capable of resolving two different regions of the flow domain, i.e. the low Reynolds number near-wall region, and the high Reynolds number outer-flow region. The presence of the two regions has significant implications for modeling the turbulence field, since the turbulence is damped near the wall and zero right at the wall. The near-wall treatment for the low-Reynolds number region also needs to be capable of including the effects of surface roughness.

The wall function technique of Launder and Spalding (1974) is the simplest way to implement wall roughness. Wall functions use empirical formulae as the boundary conditions to describe the mean velocity and turbulence quantities for the near-wall region. Therefore, there is no need to integrate model equations all the way to the wall, and most of the damping and viscous effects on turbulent flow in the near-wall region are naturally circumvented. If roughness elements are present on a solid surface, roughness parameters can be incorporated into wall functions to describe the effect of roughness on turbulence quantities. The standard wall functions are presented in Appendix A.

The two-layer $k-\varepsilon$ model is viewed as a more sophisticated approach to implement wall roughness, and is adopted in the present study. The two-layer $k-\varepsilon$ model comprises a standard $k-\varepsilon$ model and a one-equation model resolving the turbulent flow in the outer and the inner regions of the turbulent boundary layer, respectively. Durbin *et al.* (2001) introduced the concept of the hydrodynamic roughness length y_0 into the near-wall model to account for the effect of roughness on the mean flow velocity and turbulence field in the near-wall region. Details of the two-layer $k-\varepsilon$ model of Durbin *et al.* (2001) are given in chapters 2 and 3.

1.6.2 Numerical method

The finite volume method (FVM) following Patankar (1980) was used to discretize the partial differential equations and boundary conditions. The FVM obtains a set of coupled linear algebraic equations by integrating the transport equations over space and time. The discretization used a differencing scheme based on a power law relation that approximated an exponential differencing scheme. In order to determine the pressure field, the SIMPLEC algorithm was employed to solve the mass and momentum equations for the pressure-velocity fields in a segregated manner. A staggered grid was used with the SIMPLEC algorithm to avoid non-physical oscillations of the pressure field. The complete set of coupled algebraic equations was solved iteratively using alternating line solvers, and a pseudo-transient method was adopted for introducing relaxation into the solution algorithm. The convergence of the solution field was determined by assessing the residuals of the mass and momentum equations.

1.7 Thesis organization

In this dissertation, a numerical study of turbulent near-wall flow with surface roughness was carried out using a RANS-based two-layer turbulence model. The layout of the thesis consists of four chapters that include two journal manuscripts. The motivation and objectives are presented in the first chapter. Two journal manuscripts that address the objectives of the thesis are presented in chapter 2 and 3. A numerical analysis to test the performance of the two-layer $k-\varepsilon$ model of Durbin *et al.* (2001) in predicting the effect of surface roughness on the mean velocity field and turbulence quantities in both smooth and rough pipes is presented in chapter 2. Using the same two-layer $k-\varepsilon$ model, the effect of a step change in surface roughness (smooth to rough) on the mean velocity field and the turbulence quantities of a turbulent flow over a flat plate is documented in chapter 3. Chapter 4 presents a summary and conclusions drawn from the present results and an outline of future work.

1.8 References

Antonia, R. A. and Luxton, R. E., 1971. The response of a turbulent boundary layer to a step change in surface roughness Part1. Smooth to rough. *Journal of fluid mechanics*, Vol. 53, pp. 721-761.

Durbin, P. A., Medic, G., Seo, J.-M, Eaton, J. K., and Song, S., 2001. Rough wall modification of two-layer *k-ε*. *Journal of fluids engineering*, Vol. 123, pp. 16-21.

Krogstad, P.-A., and Antonia, R. A., 1999. Surface roughness effects in turbulent boundary layers. *Experiments in fluids*, Vol. 27, pp. 450-460.

Launder, B. E. and Spalding, D. B. 1974. The numerical computation of Turbulent Flows. *Computer Methods in Applied Mechanics and Engineering*, Vol. 3, pp. 269-298.

Lee, S.-H., and Sung H. J., 2007. Direct numerical simulation of the turbulent boundary layer over a rod-roughened wall. *Journal of fluid mechanics*, Vol. 584, pp. 125-146.

Lee, J. H., Sung, H. J. and Krogstad, P.-A., 2011. Direct numerical simulation of the turbulent boundary layer on a cube-roughened wall. *Journal of fluid mechanics*, Vol. 669, pp. 397-431.

Lumley, J. L. and Khajeh-Nouri, B., 1974. Computational modeling of turbulent transport. *Advances in Geophysics*, Vol. 18, pp. 169-192.

Nikuradse, J., 1933. Strömungsgesetze in rauhen Rohren. *Technical Report*, VDI-Forschungsheft 361, Berlin.

Patankar, S.V., 1980. Numerical heat transfer and fluid flow, *Hemisphere*, New York.

Patel, V.C., 1998. Perspective: flow at high Reynolds number and over rough surfaces – Achilles heel of CFD. *Journal of Fluids Engineering*, Vol. 120(3), pp. 434–444.

Pendergrass, W. and Arya S. P. S., 1984. Dispersion in neutral boundary layer over a step change in surface roughness – 1. Mean flow and turbulence structure. *Atmospheric Environment*, Vol. 18, pp. 1267-1279.

Rao, K.S., Wyngaard, J. C., and Cote, O. R., 1973. The structure of the two-dimensional internal boundary layer over a sudden change of surface roughness. *Journal of the Atmospheric Sciences*, Vol. 31, pp. 738-746.

Savelyev S. A. and Taylor P. A., 2005. Internal boundary layers: 1. Height formulae for neutral and diabatic flows. *Boundary-Layer Meteorology*, Vol. 115, pp. 1-25.

Versteeg, H., and Malalasekra, W., 2011. An introduction to computational fluid dynamics-*The finite volume method, 2nd edition*. India: Pearson Education, Ltd

CHAPTER TWO

PREDICTION OF TURBULENT FLOW IN A ROUGH PIPE USING A NEAR-WALL RANS MODEL

Publication:

An earlier and briefer version of this manuscript was presented at the following conference:

Chu, M. and Bergstrom, D. J., Prediction of turbulent flow in a rough pipe using a near-wall RANS model, 25th Annual CFD Society of Canada Conference: CFDSC 2017, University of Windsor, June 18 – June 20.

Preamble

The research work presented in this chapter focuses on the first objective of the thesis. This chapter documented the numerical results obtained for turbulent flow through a rough pipe using the two-layer $k-\varepsilon$ model developed by Durbin *et al.* (2001), with special attention to the effects of roughness on the mean flow and turbulence fields for the smooth, transitionally-rough, and fully-rough flow cases in the region very close to the wall. This information is typically absent in the previous studies which use this model.

Abstract

The present paper studies fully developed turbulent flow of an incompressible, viscous fluid in a vertical pipe. Three different flow cases, i.e. smooth, transitionally rough, and fully rough, under a constant pressure gradient of $dp/dx = 642$ Pa/m were simulated based on the two-layer $k-\varepsilon$ model by Durbin *et al.* (2001). In their model, the concept of a hydrodynamic roughness length y_0 was introduced to account for the effect of wall roughness on the mean flow properties. The predictions for the mean velocity, eddy viscosity, Reynolds shear stress, turbulence kinetic energy, and energy budget were compared for the different roughness conditions. The two-layer model correctly predicted the downward shift of the mean velocity profile in the overlap region due to the roughness. It also predicted that the effect of roughness is to enhance the level of the eddy viscosity in the region next to the wall under a constant pressure gradient. In the outer region, the same level of turbulent viscosity was approximated at lower bulk flow rates. Of special interest are the predictions for the turbulence field very close to the wall. In this region, the wall roughness results in finite values of the Reynolds shear stress and turbulence kinetic energy at the wall.

Keywords – RANS, two-layer $k-\varepsilon$ model, boundary layer, roughness

2.1 Introduction

Turbulent flow is the flow regime most often encountered in engineering applications, such as oil pipelines and flow over aircraft. Often these flows are over walls, in which case surface roughness can be present, e.g., rust growing on the interior surface of a pipe or icing on an airfoil. The accurate prediction of the effects of wall roughness on turbulent flow and heat transfer is of great interest to engineers. For computational predictions which use a Reynolds Averaged Navier-Stokes (RANS) formulation, the turbulence model for the Reynolds stress needs to be modified in the near-wall region to account for the effect of wall roughness. In 1998, Patel identified modeling high Reynolds number flows over rough surfaces as a significant challenge for computational fluid dynamics (CFD). Twenty years later, this assessment is still valid.

Recall that Nikuradse (1933) originally introduced the concept of equivalent sand-grain roughness to characterize rough surfaces. Using the concept of sand-grain roughness height, Durbin *et al.* (2001) modified a two-layer $k-l$ model to account for the effect of wall roughness on a turbulent wall-boundaed flow. Suga *et al.* (2006) proposed an analytical wall function for capturing the behavior of turbulent flow over rough walls. Jackson (1981), working from the meteorological point of view, modelled the effect of wall roughness by incorporating roughness-related geometric parameters into the logarithmic law. White *et al.* (1996) proposed a new low-Reynolds-number $k-\varepsilon$ model for predicting turbulent flow over rough surfaces, in which the equivalent sand-grain roughness height was used. Aupoix and Spalart (2003) modified the Spalart-Allmaras turbulence model to account for wall roughness. A recent paper by Knopp *et al.* (2009) developed a new formulation of the $k-\omega$ turbulence model to account for wall roughness, also based on the equivalent sand-grain roughness approach. Their model formulation addressed the problem of the need for a very fine near-wall mesh resolution and inaccurate predictions of skin friction for transitionally rough surfaces associated with the original shear-stress transport (SST) model. Eça and Hoekstra (2011) and Hellsten and Laine (1997) also considered modelling of rough walls using the SST turbulence model. The current study adopted the two-layer turbulence model of Durbin *et al.* (2001) for two reasons: first, the turbulence model has been shown to perform well in boundary-layer flows, and second, the two-layer model of Durbin *et al.* (2001) is relatively easy to implement and potentially allows itself to be calibrated for different types of roughness.

The objective of this study is to utilize the two-layer $k-\varepsilon$ turbulence model developed by Durbin *et al.* (2001) to explore the effect of wall roughness on turbulent flow in fully developed pipe flow. A specific contribution of the paper was to explore the prediction of the turbulence field in the immediate vicinity of the roughness, which was generally missing from the previous studies. The paper is organized as follows: section 2.2 reviews the two-layer $k-\varepsilon$ model. Section 2.3 discusses the flow and the numerical method adopted. In Section 2.4, the results predicted by the two-layer $k-\varepsilon$ model are presented, and some conclusions are drawn in Section 2.5.

2.2 The two-layer $k-\varepsilon$ model

2.2.1 Governing equations

In the present study, the streamwise momentum equation using a RANS formulation is solved together with transport equations for the turbulence kinetic energy and its dissipation rate. For steady incompressible, fully developed turbulent flow through a round pipe with no swirl, the radial and azimuthal velocity components are zero. Gravitational forces are neglected. The simplified RANS equation in the streamwise direction can be written as follows using a cylindrical coordinate system:

$$0=-\frac{1}{\rho}\frac{\partial P}{\partial z}+\frac{1}{r}\left(\nu\frac{dU_z}{dr}-<u_z u_r>\right)+\frac{d}{dr}\left(\nu\frac{dU_z}{dr}-<u_z u_r>\right), \tag{2.1}$$

where < > represents time-averaging. In equation (2.1), r is the radial coordinate and z is in the streamwise coordinate, while the symbol U_z represents the mean velocity component in the radial direction. $<u_z u_r>$ is the unknown Reynolds stress term in equation (2.1). For future reference, note that y measures the wall-normal distance, and can be represented by $y=R-r$, where R represents the pipe radius. As written, equation (2.1) is not closed, which then requires specification of a turbulence model for the Reynolds shear stress term.

The two-layer $k-\varepsilon$ model combines the high-Reynolds number form of the $k-\varepsilon$ model with the $k-l$ model for the region next to the wall. At the patching point, the two-layer formulation

switches abruptly from the $k-l$ model to the $k-\varepsilon$ model. Noting that the unsteady and convective terms are zero, then the transport equations for the turbulence kinetic energy k and its dissipation rate ε can be written as follows:

$k\ equation$

$$0 = D_k + P_k - \varepsilon, \tag{2.2}$$

$\varepsilon\ equation$

$$0 = D_\varepsilon + P_\varepsilon - C_{\varepsilon 2}\frac{\varepsilon^2}{k}, \tag{2.3}$$

The diffusion and production terms in equations (2.2) and (2.3) respectively, are defined as follows:

$$D_k = \frac{1}{r}\frac{\partial}{\partial r}\left[r\left(\nu + \frac{\nu_t}{\sigma_k}\right)\frac{\partial k}{\partial r}\right], \tag{2.4}$$

$$P_k = \nu_t\left(\frac{\partial U_z}{\partial r}\right)^2, \tag{2.5}$$

$$D_\varepsilon = \frac{1}{r}\frac{\partial}{\partial r}\left[r\left(\nu + \frac{\nu_t}{\sigma_\varepsilon}\right)\frac{\partial \varepsilon}{\partial r}\right], \tag{2.6}$$

$$P_\varepsilon = C_{\varepsilon 1}\frac{\varepsilon}{k}P_k, \tag{2.7}$$

where ν and ν_t are the molecular and turbulent kinematic viscosity, respectively, with constants $\sigma_k = 1.00$, $\sigma_\varepsilon = 1.30$, $C_{\varepsilon 1} = 1.44$, *and* $C_{\varepsilon 2} = 1.92$. Using the Boussinesq eddy viscosity relationship the Reynolds shear stress can be written as follows:

$$-< u_z u_r >= \nu_t \frac{\partial U_z}{\partial r}, \tag{2.8}$$

In equation (2.8), ν_t has the dimensions $[\mathrm{m}^2/\mathrm{s}]$, and can be expressed as the product of a turbulent velocity scale v (m/s) and a turbulent length scale l (m). Then ν_t can be modelled as follows:

$$\nu_t = C_\nu v l, \tag{2.9}$$

where $C_\nu = 0.09$ is a dimensionless constant. For the $k-\varepsilon$ model, l and v are related to k and ε using the following relations:

$$l = k^{3/2}/\varepsilon, \tag{2.10}$$

$$v = k^{1/2}. \tag{2.11}$$

Therefore, ν_t for the $k-\varepsilon$ model is specified by

$$\nu_t = C_\nu k^2/\varepsilon. \tag{2.12}$$

In the $k-l$ model, equations (2.9) and (2.10) are modified to incorporate the effect of the wall on the eddy viscosity and the dissipation rate as follows:

$$\nu_t = C_\nu \sqrt{k} l_\nu, \tag{2.13}$$

$$\varepsilon = k^{3/2}/l_\varepsilon. \tag{2.14}$$

In equations (2.13) and (2.14), l_ε and l_ν are length scales that each incorporate a Van Driest damping function, i.e.

$$l_\varepsilon = C_l y_{\text{eff}}\left(1 - e^{-R_y/A_\varepsilon}\right), \tag{2.15}$$

$$l_\nu = C_l y_{\text{eff}}\left(1 - e^{-R_y/A_\nu}\right), \tag{2.16}$$

where $C_l = 2.5,\ A_\varepsilon = 2C_l = 5.0$, and $R_y = y_{\text{eff}}\sqrt{k}/\nu$ is a Reynolds number based on the effective wall-normal distance y_{eff}. The definition of y_{eff} is presented below. A_ν is a constant (depends on the flow regime). The $k - l$ model governs the flow behavior in the region next to the wall, and switches to the $k - \varepsilon$ model at the patching point, i.e. $1 - e^{-R_y/A_\nu}$ is equal to 0.95. This condition applies for both smooth and rough flow cases.

2.2.2 The effect of roughness

Durbin *et al.* (2001) defined the location of the y-origin as where the mean velocity is extrapolated to zero, e.g. $U_z(y = 0) = 0$. The origin of $y = 0$ is located right on the wall surface for a smooth wall flow. For a rough surface, the concept of hydrodynamic roughness length y_0 is introduced to capture the effect of surface roughness on the turbulent boundary layer. The value of the dimensionless form of y_0 was determined using the calibration curve given in Durbin *et al.* (2001). With the concept of y_0, the effective wall-normal coordinate y_{eff} can be defined as follows:

$$y_{\text{eff}} = y + y_0. \tag{2.17}$$

In the paper by Durbin *et al.* (2001), the location of y_{eff} relative to the roughness is not specifically discussed. Based on the discussion above, the geometric relationship between y_{eff} and a generic roughness is shown schematically in Figure 2.1. From Figure 2.1, the origin of y is typically located a short distance d below the top of the roughness elements. Meanwhile, the origin of y_{eff}

is located somewhat below the origin of y by a distance of y_0. The mean velocity profile is assumed to satisfy the following relation in the near-wall region under fully rough conditions:

$$U_z = (u_\tau/\kappa) ln[(y + y_0)/y_0]. \quad (2.18)$$

In equation (2.18), u_τ is the friction velocity, defined as $(\tau_w/\rho)^{1/2}$, and the value of von Karman's constant is $\kappa = 0.41$. From equation (2.18), the mean velocity is equal to zero at $y = 0$. In atmospheric boundary layer modeling, the mean velocity profile over a rough wall is given by $U_z = u_\tau/\kappa(y/z_0)$, where z_0 is called the hydrodynamic roughness length. Note y_0 and z_0 are not same variable.

In the present paper, the concept of the equivalent sand-grain roughness k_{sg} (m) is adopted: k_{sg} has its non-dimensional form using inner coordinates as $k_{\mathrm{sg}}^+ = k_{\mathrm{sg}} u_\tau/\nu$. By definition, a hydraulically smooth wall occurs for $k_{\mathrm{sg}}^+ < 5$; a transitionally rough flow occurs for $5 \le k_{\mathrm{sg}}^+ \le 70$; and a fully rough flow occurs for $k_{\mathrm{sg}}^+ > 70$. As k_{sg}^+ increases, the damping effect due to the wall is reduced, which then requires the value of l_ν in equation (2.16) to be adjusted accordingly. The linear interpolation by Durbin *et al.* (2001)

$$A_\nu = \max[1, A_\nu^0(1 - k_{\mathrm{sg}}^+/90)] \quad (2.19)$$

is specified to implement the damping effect of the roughness. The smaller A_ν becomes, the weaker the damping felt by the flow. For the dissipation rate, $A_\varepsilon = 5.0$ in equation (2.15) is small enough to have little damping effect on fully rough flows. The boundary condition for k on a smooth wall is $k(y = 0) = 0$. For a rough wall, a quadratic interpolation for the boundary condition for k is introduced, i.e.

$$k(y=0) = \frac{u_\tau^2}{\sqrt{C_\nu}} min\left[1, \left(\frac{k_{sg}^+}{90}\right)^2\right], \tag{2.20}$$

while the boundary condition for ε is defined as

$$\varepsilon(y=0) = \nu k(0) A_\varepsilon / y_0^2 \, C_l. \tag{2.21}$$

Equation (2.20) and (2.21) show that for a rough wall both k and ε have a finite value at $y = 0$. Note that for an eddy viscosity model, the turbulent viscosity is finite at $y = 0$ where $U_z = 0$.

2.3 Flow description and numerical method

In the present study an in-house CFD code was used to solve the case of steady, incompressible, fully developed turbulent pipe flow based on a RANS formulation. The fluid was assumed to be water, with density $\rho = 1000$ kg/m^3 and kinematic viscosity $\nu = 1.5 \times 10^{-5}$ m^2/s. The axial pressure gradient remained at a constant value of $dp/dx = 642$ Pa/m for all three flow cases, i.e. smooth, transitionally rough, and fully rough. The values of $y_0 = y_0^+ \nu / u_\tau$ were calculated to be 2.94×10^{-5} m and 2.52×10^{-5} m for the transitionally-rough and fully-rough flow cases, respectively.

A circular cylindrical coordinate system $(r, \theta, z)$was used to define the flow geometry, as shown in Figure 2.2. The pipe radius was $R = 0.026$ m. The solution domain consisted of a radial section bounded by the centerline and wall of the pipe. More specifically, the grid was refined at the wall to resolve the steep velocity gradients in this region. A non-uniform grid of 81 control volumes was sufficient to obtain a grid independent solution. An in-house Fortran code was developed to solve this problem so that the details of the wall treatment were completely transparent. The transport equations were discretized using the finite volume method. The spatial differencing scheme was second-order and a pseudo-transient formulation was used to iterate the solution fields until convergence was obtained. The final residuals for the U, k, and ε transport equations were

approximately 10^{-7}. A no-slip condition was used for the mean velocity at the wall, while a symmetry condition was used at the centerline. The specific boundary conditions for the k and ε equations were given in the previous section. The grid was refined such that the location of the first interior node ($i = 2$) next to the wall was located at $y^+ = 0.1$, for both the smooth and rough flow scenarios.

2.4 Results and discussion

2.4.1Mean velocity profile

Three characteristic flow regimes were considered: hydraulically smooth, transitionally rough, and fully rough. Figure 2.3 shows a set of mean velocity profiles obtained using the two-layer $k - \varepsilon$ model. For the smooth, transitionally rough and fully rough cases, the values of the equivalent sand-grain roughness were $k_{sg}^+ = 0$, $k_{sg}^+ = 23$, and $k_{sg}^+ = 110$, respectively. The log-law, given by

$$\frac{U_z}{u_\tau} = \left(\frac{1}{\kappa}\right) \ln\left(\frac{y u_\tau}{\nu}\right) + B + \Delta U_z^+, \tag{2.22}$$

is also included in Figure 2.3 for comparison. For the case of the smooth wall flow, the additive constant used in the log-law was $B = 5.0$, and $\Delta U_z^+ = 0$. Also included is the DNS data for smooth pipe flow by Wu and Moin (2008) for a Reynolds number of $Re_d = 5300$ based on the diameter and bulk velocity. The velocity profiles shown in Figure 2.3 were plotted using inner-coordinates and the effective wall-normal distance, y_{eff}, which includes a small shift of the y-origin to include the effect of roughness (as described in section 2.2.2). For the smooth-wall case, the mean velocity profile matches the canonical logarithmic velocity profile in the overlap region ($30 < y^+ < 500$) and includes a distinct wake effect in the outer region. The prediction for the smooth pipe also agrees well with the DNS data, although the predicted value of U_z^+ was slightly larger than the DNS data in the log-layer for $60 < y_{\text{eff}}^+ < 200$. The characteristic effect of roughness is a downward shift of the mean velocity profile compared to the smooth-wall case. In

addition, the roughness causes the viscous transport in the region next to the wall to become insignificant. For the fully rough case, i.e. $k_{sg}^{+} = 110$, the velocity profile remains almost logarithmic up to the wall. In the region next to the wall, the fully rough profile deviates upward away from the log-law, and this discrepancy tends to reduce with the increase in roughness. The cross between the predicted profiles for the fully-rough and the transitionally-rough flow cases is the reflection of the concept of hydrodynamic roughness length.

2.4.2 Roughness shift

Figure 2.4 shows the roughness shift ΔU_z^+ as a function of the equivalent sand-grain roughness. Also shown are two empirical relations: the Prandtl-Schlichting (1979) relation for the fully rough case and the value of the roughness shift for the transitionally rough case based on the sand-grain data of Nikuradse (1933). Note that for a hydraulically smooth surface the roughness shift is by definition equal to zero, i.e. $\Delta u_z^+ = 0$. In general, the roughness shift increases with an increase in the surface roughness. For $k_{sg}^{+} \geq 70$, i.e. for fully rough flow, the predicted values of ΔU_z^+ agree well with the Prandtl-Schlichting relation (1979). As the equivalent sand-grain roughness decreases and viscous effects begin to be significant, the roughness shift departs from the Prandtl-Schlichting relation (1979). For $k_{sg}^{+} \leq 70$, the predicted values of Δu_z^+ agree well with the experimental data obtained by Nikuradse. The behavior above is consistent with the fact that the value of y_0 was calibrated by Durbin *et al.* (2001) to match the sand-grain data of Nikuradse.

2.4.3 Mean velocity gradient

Wu and Moin (2008) provided an insightful analysis of the mean velocity gradient based on their DNS study of turbulent pipe flow; a similar analysis is presented here based on the RANS prediction. The normalized mean velocity gradient with respect to the radial coordinate is shown in Figure 2.5 for the smooth flow and rough flow cases with $k_{sg}^{+} = 23$ and 110.

The mean velocity gradient dU_z^+/dy^+ for the smooth wall exhibits a convex-to-concave change in curvature, as it continuously decreases with y_{eff}/R, from a peak value in the immediate vicinity of the wall to a value of zero at the pipe centerline. For the smooth wall case, in the region $y_{\text{eff}}/R <$

0.002, which lies within the viscous sublayer, dU_z^+/dy^+ remains constant at a value of unity due to the fact that $U_z^+ = y^+$, which is reflected as a plateau in Figure 2.5. This plateau coincides with the curved segment of the smooth-wall mean velocity profile for $y_{\text{eff}}^+ < 5$ in Figure 2.3.

In comparison to the smooth wall flow, the value of $\mathrm{d}U_z^+/\mathrm{d}y^+$ for the rough flow cases with $k_{\text{sg}}^+ = 23$ and $k_{\text{sg}}^+ = 110$ do not show a plateau next to the wall, since the viscous sublayer is disrupted by the roughness elements. For $k_{\text{sg}}^+ = 23$, the flow is transitionally rough, the viscous sublayer is only partly disrupted and a convex curvature can still be observed in Figure 2.5. Although the profile of dU_z^+/dy^+ shifts slightly downward, the overall profile still retains the shape of the smooth flow case. On the other hand, a significant reduction in the value of dU_z^+/dy^+ at the wall can be observed for $k_{\text{sg}}^+ = 110$ when the viscous sublayer is fully disrupted. The region of convex curvature disappears for the fully rough flow. For $k_{\text{sg}}^+ = 110$, the behavior of dU_z^+/dy^+ in the range $\mathrm{y}_{\text{eff}}/R < 0.02$ no longer matches the smooth flow profile. For the fully rough flow, the turbulent shear stress is non-zero at the wall, so that the normalized mean velocity gradient is less than unity. In addition, Figure 2.5. shows that in the region next to the wall the profile of dU_z^+/dy^+decreases more rapidly for the smooth and the transitionally-rough flow case ($k_{\text{sg}}^+ = 23$), as compared to the fully-rough flow case ($k_{\text{sg}}^+ = 110$). In the outer region, i.e. for $y_{\text{eff}}/R > 0.1$, dU_z^+/dy^+ decreases for all three different flow cases, which collapse onto a single curve at the pipe centerline. For all flow regimes, the gradient of velocity becomes very small near the centerline of the channel.

2.4.4 Eddy viscosity

The radial profile of the eddy viscosity normalized with the molecular viscosity, is shown in Figure 2.6 a) and b) for the smooth and rough surfaces. Figure 2.6 a) indicates that the value of the normalized eddy viscosity, ν_t/ν, increases in a decreasing manner with y_{eff}/R. Far away from the wall, the value of the dimensionless eddy viscosity is slightly larger for the rough flow cases than for the smooth wall case. The eddy viscosity is largest for the fully rough flow, however, the discrepancy between the smooth and rough flow cases is relatively small. Recall that the axial pressure gradient is maintained the same for all three flow cases, so that the bulk flow rate

decreases for the rough-wall cases. This implies that the rough-wall flows produce approximately the same level of turbulent viscosity at lower bulk flow rates or Reynolds number.

In the immediate vicinity of the wall, the value of ν_t/ν is relatively small for the smooth and transitionally-rough flow cases, but significant for the fully-rough flow case, as can be seen from Figure 2.6 b). The values of ν_t/ν at the first node above the wall, denoted $\nu_t(2)/\nu$, are given in Table 2.1. For the smooth wall case, the value is negligible. For the transitionally rough flow, the value is larger, but still close to zero. For the fully rough flow, the value is approximately 95 percent of the molecular value, and not negligible. This behavior is consistent with the notion that for a fully rough flow, the turbulence is non-zero at the crest of the roughness elements.

2.4.5 Reynolds shear stress

The radial profile for the normalized Reynolds shear stress for the smooth and rough flow cases, together with the DNS data of Wu and Moin (2008) for a smooth pipe flow at $Re_d = 44000$, is shown in Figure 2.7 a) and b). Figure 2.7 a) shows that $-< u_z u_r >^+$ exhibits the well-known near-wall peak value for all three flow cases, as does the DNS profile. For the smooth flow case, the predicted profile for $-< u_z u_r >^+$ has a peak value that is greater than for the DNS data of Wu and Moin (2008). This can be explained by the larger Reynolds number used in the present study, i.e. $Re_d = 101770$ compared to $Re_d = 44000$. For $y_{\text{eff}}/R > 0.1$, $-< u_z u_r >^+$decreases monotonically, with the four different curves collapsing onto a single curve. This is consistent with Townsend's near-wall similarity hypothesis, which suggests that when properly scaled, the Reynolds shear stress profile in the outer region is not affected by surface roughness. However, it is also clear that close to the wall, the peak value of the normalized Reynolds shear stress is largest for the fully rough case, the value being almost 3 percent more than the smooth-wall case.

Figure 2.7 b) was created to deliberately expand the region next to the wall ($y_{\text{eff}}/R < 0.1$) by using a logarithmic scale for y_{eff}/R. Figure 2.7 b) shows that the different profiles for $-< u_z u_r >^+$ each exhibit distinct behavior from each other within the region $y_{\text{eff}}/R < 0.1$. As noted above, all profiles exhibit a near-wall peak, with the peak values for the rough cases being larger than for the smooth case. Moreover, a trend that the peak value tends to increase with the increasing value of k_{sg}^+ can be observed in Figure 2.7 a) and b). In addition, the predicted

transitionally rough profile lies slightly above the smooth-wall profile, however the overall shape retains that of the smooth profile. On the other hand, the predicted profile for the fully rough flow exhibits an abrupt jump at the first node above the wall, with the overall profile lying above both the transitionally-rough and the smooth profile by a significant amount. For the rough flow cases, the shear stress profiles exhibit finite values very close to the wall, whereas the smooth wall profile reduces to zero at the wall. In Figure 2.7 b), at the first node above the wall, the value of $-< u_z u_r >^+$ is close to zero for the smooth and the transitionally rough flow case ($k_{sg}^+ = 23$), but jumps to a much larger value of approximately 0.43 for the fully rough case ($k_{sg}^+ = 110$).

2.4.6 Turbulence kinetic energy

The radial profiles of the normalized turbulence kinetic energy for the smooth and rough cases ($k_{sg}^+ = 23$, and $k_{sg}^+ = 110$) are presented in Figure 2.8 a) and b). Figure 2.8 a) shows that for all profiles, k^+peaks in the region next to the wall, and that the effect of roughness is to slightly reduce the peak value. In the region beyond $y_{\text{eff}}/R > 0.1$, k^+ becomes indistinguishable for all three flow cases, collapsing onto a single curve that reduces steadily toward the centerline, although the fully-rough flow profile sits slightly above the smooth and the transitionally-rough profiles. Figure 3.8 b) expands the near-wall region by using a logarithmic scale for y_{eff}/R. For the smooth wall, the turbulence kinetic energy reduces to zero as the wall is approached. Unlike the smooth flow case, for the rough flow cases the turbulence kinetic energy retains a finite value at the wall. The values of k^+ at the first node above the wall are 0.3 and 3.3, respectively, for the transitionally-rough ($k_{sg}^+ = 23$) and the fully-rough flow ($k_{sg}^+ = 110$). The shapes of the near-wall profiles for the transitionally-rough flow and the smooth flow are somewhat similar. On the other hand, k^+ for the fully-rough flow case at $k_{sg}^+ = 110$ exhibits a local minimum next to the wall, and then increases to a second peak value at the wall.

2.4.7 Energy budget

For fully developed pipe flow, the turbulence kinetic energy transport equation (equation 2.2) can be analysed in terms of the balance between three different terms: diffusion, production and

dissipation. The predictions for the normalized turbulence production and viscous dissipation rates, denoted by P^+ and ε^+, are presented in Figure 2.9. Recall that the turbulence production extracts energy from the mean flow, while the dissipation rate denotes the conversion of turbulence kinetic energy to thermal energy at the smallest scales due to viscous effects. Also included is the DNS data ($Re_\tau = u_\tau R/\nu = 1000$) for smooth-wall pipe flow from El Khoury *et al.* (2013) for a Reynolds number based on the friction velocity of $Re_\tau = 2370$. The value of P^+ reduces to zero at the first node above the wall, i.e. $P^+(2) = 0$. This can be explained by the fact that $\nu_t(2) = 0$ for the smooth flow case, indicating no turbulence is produced right at the wall surface. In Figure 2.9, the predicted P^+ profile agrees very well with the DNS data throughout the entire boundary layer for the smooth flow case. The predicted smooth P^+ profile peaks in the region very close to the wall, i.e. $y^+_{\text{eff}} \sim 10$ ($y_{\text{eff}}/R \sim 0.047$). The predicted P^+ profile for the transitionally-rough flow retains the shape of the smooth profile across the pipe. For the fully-rough flow case, P^+ peaks at the first node above the wall, and decreases in a diminishing manner moving away from the wall. For $y^+_{\text{eff}} > 30$ ($y_{\text{eff}}/R \sim 0.014$), the predicted P^+ profiles for all three flow cases collapse onto a single curve.

For the smooth flow, ε^+agrees well with the DNS data for $y^+_{\text{eff}} > 30$. For $y^+_{\text{eff}} < 30$, the predicted ε^+ peaks very close to the wall at $y^+_{\text{eff}} \sim 10$, however the DNS exhibits a peak of ε^+ at the wall itself. The predicted value of ε^+ is finite at the first node above the wall for the smooth flow case. This behavior is indicative of the well-known failure of many low Reynolds number model formulations to correctly predict the dissipation rate profile very close to the wall.

For the transitionally-rough flow, the ε^+ profile retains the shape of the smooth-wall case throughout the entire pipe, although at the first node above the wall ε^+ sits slightly higher than the smooth-wall case. For the fully-rough flow, ε^+ peaks at the first node above the wall, and then drops rapidly as y^+_{eff} increases. The peak value of $\varepsilon^+$for the fully-rough case is much greater than that for the smooth wall. For $y^+_{\text{eff}} > 30$, the predicted ε^+ profiles for all three flow cases collapse onto a single curve. The role of the diffusion term (not shown in Figure 2.9) is to transport turbulence kinetic energy into the region near the wall to balance the dissipation rate in the absence of any local production.

2.4.8 Darcy friction factor

From an engineering perspective, perhaps the most important flow parameter is the friction drop typically given in terms of the Darcy friction factor. The values of the Darcy friction factor for the different surface roughness conditions predicted by the two-layer $k-\varepsilon$ model are shown in Table 2.2 and denoted by f^{code}. The values of the Darcy friction factor calculated using the empirical correlation by Colebrook (2011), denoted by f^{emp}, are also shown**.** Comparing f^{code} with f^{emp}, the percentage differences for $k_{sg}^{+}=0$, $k_{sg}^{+}=23$, and $k_{sg}^{+}=110$ were calculated to be 3.35%, 16.7%, and 9.71% , respectively. The differences are relatively small for the smooth and fully-rough flows, but relatively large for the transitionally-rough flow. Note that the Colebrook relationship is an interpolation between the smooth and fully-rough cases, and the estimates for the transitionally-rough flow cases are expected to show the most uncertainty.

2.5 Conclusions

Steady, incompressible, fully developed turbulent pipe flow for $dp/dx = 642$ Pa/m has been investigated using the two-layer $k-\varepsilon$ model for the case of smooth, transitionally-rough and fully-rough flow. On a log-law plot, the wall roughness causes a downward shift in the mean velocity profile, which varies with the degree of roughness. The numerical results for the roughness shift were generally in good agreement with the experimental correlations for the transitionally-rough and the fully-rough flows. The mean velocity gradient for the three different flows revealed significant differences. The peak value of the normalized mean velocity gradient for the smooth flow case is approximately equal to the transitionally-rough case, however larger than the fully-rough flow case. An obvious plateau in the region of $y/R < 0.001$ can be observed for the smooth flow case, implying an uninterrupted viscous sublayer. For the rough flow cases, the mean velocity gradient is generally smaller due to the partially or fully disrupted viscous sublayer. For the same pressure gradient, the eddy viscosity profiles predicted for all three flows were approximately the same; however, the fully rough flow was characterised by a large finite value at the wall. The Reynolds shear stress peaks near the wall for all three flow cases, with a slightly larger peak value for the rough-wall cases. Furthermore, for the fully rough flow, the Reynolds shear stress has a large finite value at the wall. The turbulence kinetic energy also peaks

near the wall for all three flow cases, but in this case the effect of roughness is to slightly decrease the peak value. Whereas the turbulence kinetic energy reduces to zero at the wall for the smooth flow, the wall value remains finite for the rough-wall cases. For the fully rough flow case, there are two peaks generated within the region $y_{\text{eff}}/R < 0.1$: one right at the wall, and another at $y_{\text{eff}}/R = 0.1$. Finally, both the production and dissipation peak in the region next to the wall for all three flow cases. For the smooth flow case, the value of production is zero at the wall, while the dissipation rate exhibits a finite value. For the transitionally-rough flow case, both the production and dissipation profiles retain the shape of the smooth-wall profile. For the fully-rough flow case, both production and its dissipation rate exhibit a peak at the wall surface, with the peak value of the dissipation 6.5 times larger than that of the production. Comparison of the values of the Darcy friction factor predicted by the model and the Colebrook (2011) correlation indicate good agreement for the smooth and the fully-rough flow cases, with a relatively larger error for the transitionally-rough flow case.

Overall the contribution of this study has been to document the behavior of a RANS model very close to the rough surface, and compare the way in which the turbulence properties predicted for a smooth-wall and a rough-wall turbulent flow go to the wall. Experimental and DNS studies are required to document the mean and turbulence fields in close proximity to the roughness elements.

2.6 References

Aupoix, B. and Spalart, P. R., 2003. Extensions of the Spalart–Allmaras turbulence model to account for wall roughness. *International Journal of Heat and Fluid Flow*, Vol. 24, pp. 454–462.

Durbin, P. A., Medic, G., Seo, J.-M, Eaton, J. K., and Song, S., 2001. Rough wall modification of two-layer *k-ε*. *Journal of Fluids Engineering*, Vol. 123, pp. 16-21.

EI Khoury, G. K., Schlatter, P., Noorani, A., Paul, F., Fischer, P.F., Brethouwer, G. and Johansson, A.V., 2013. Direct numerical simulation of turbulent pipe flow at moderately high Reynolds numbers. *Flow Turbulence Combust*, Vol. 91, pp. 475-495.

Eça, L., and Hoekstra, M., 2011. Numerical aspects of including wall roughness effects in the *SST k-ω* eddy viscosity turbulence model. *Computers & Fluids*, Vol. 40, pp. 229-314.

Hellsten, A., and Laine, S., 1997. Extension of the *k-ω-SST* turbulence model for flows over rough surfaces. *AIAA Journal*, Vol. 36(9), PP. 1997-3577.

Jackson, P. S., 1981. On the displacement height in the logarithmic velocity profile. *Journal of Fluid Mechecanics*, Vol. 111, pp. 15-25.

Knopp, T., Eisfeld, B., and Calvo, J. B., 2009. A new extension for *k-ω* turbulence models to account for wall roughness. *Journal of Fluid Engineering*, Vol. 118, pp. 255-259.

Nikuradse, J., 1933. Strömungsgesetze in rauhen Rohren. *Technical Report*, VDI-Forschungsheft 361, Berlin.

Patel, V.C., 1998. Perspective: flow at high Reynolds number and over rough surfaces – Achilles heel of CFD. *Journal of Fluids Engineering*, Vol. 120(3), pp. 434–444.

Schlichting, H., 1979. *Boundary-Layer Theory, 7th edition*. New York: McGraw-Hill.

Suga, K., Craft, T.J., and Iacovides, H., 2006. An analytical wall-function for turbulent flows and heat transfer over rough walls. *International Journal of Heat and Fluid Flow*, Vol. 27, pp. 852–866.

Versteeg, H., and Malalasekra, W., 2011. An introduction to computational fluid dynamics-*The finite volume method, 2nd edition*. India: Pearson Education, Ltd

Wu, X., and Moin, P., 2008. A direct numerical smulation study on the mean velocity characteristics in turbulent pipe flow. *Journal of Fluid Mechanics*, Vol. 608, pp. 81-112.

Zhang, H. Z., Faghri, M., and White, F., 1996. A New Low-Reynolds-Number k-epsilon Model for Turbulent Flow over Smooth and Rough Surfaces. *Journal of Fluids Engineering*, Vol. 118, pp. 255-259.

Table 2.1. ν_t/ν at the first grid node

Flow cases	$y^+_{eff}(2)$	ν_t/ν
Smooth	0.0992	$1.37E-8$
Transitionally rough ($k^+_{sg}=23$)	2.800	0.00949
Full rough ($k^+_{sg}=110$)	2.399	0.949

Table 2.2. Comparison of Darcy friction factor

k^+_{sg}	Re_d	f^{code}	f^{emp}
smooth	101770	0.0173	0.0179
23	85218	0.0252	0.0310
110	61862	0.0465	0.0515

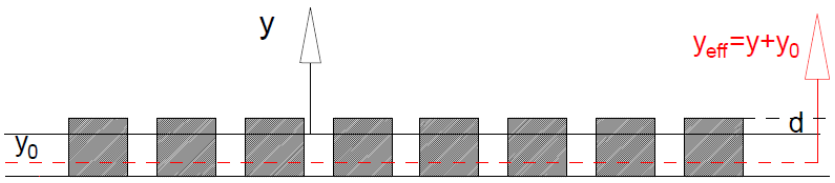

Figure 2.1. Schematic of y_{eff} and y_0 relative to the roughness elements.

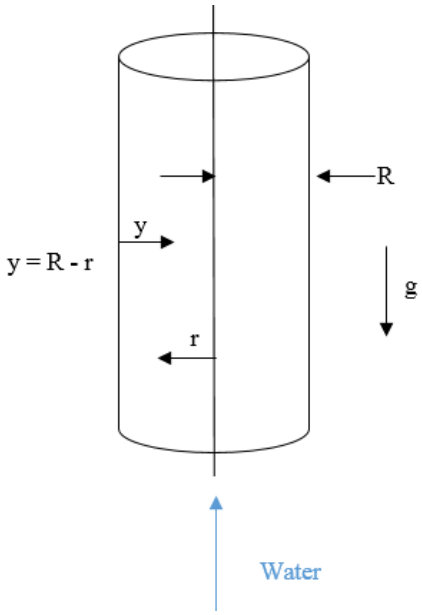

Figure 2.2. Schematic of the flow geometry

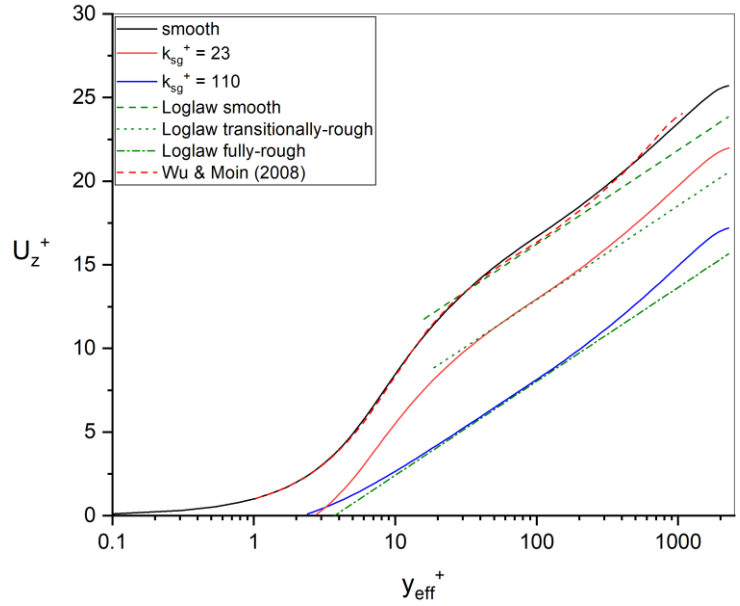

Figure 2.3. Mean velocity profiles using inner coordinates

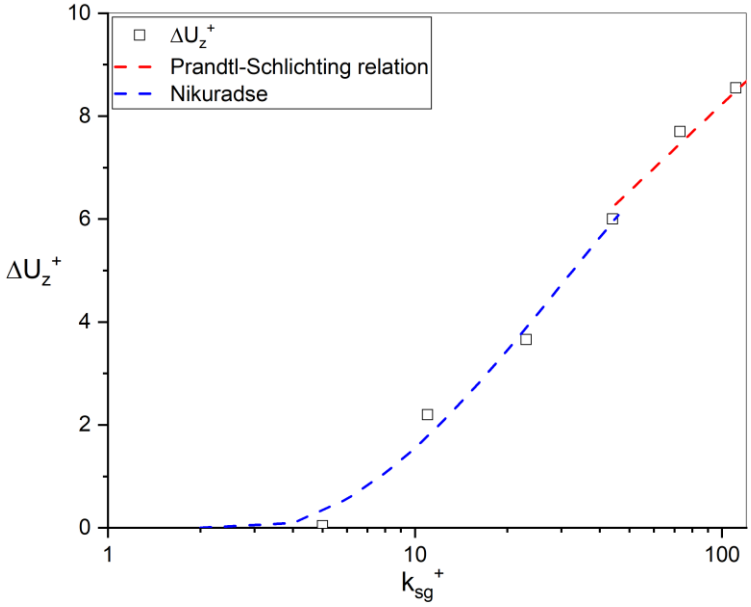

Figure 2.4. Roughness shift as a function of equivalent sand-grain roughness

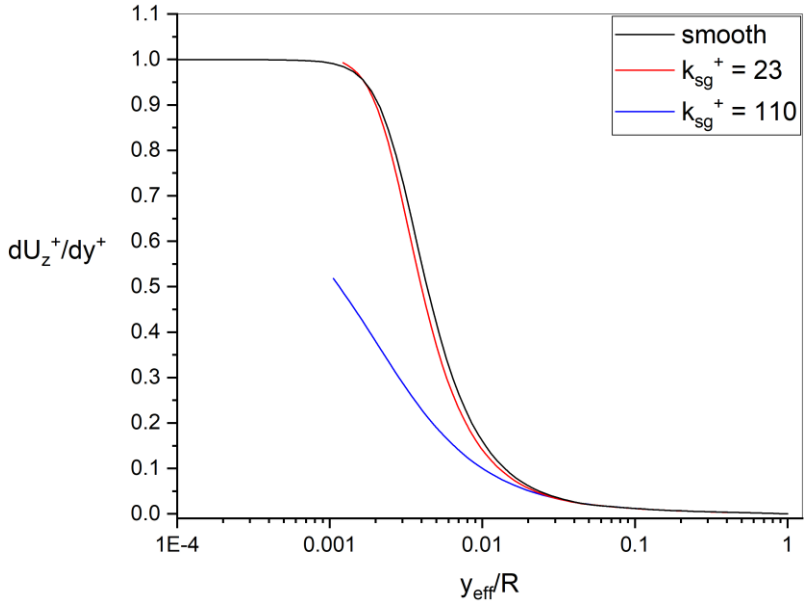

Figure 2.5. The profile of normalized mean velocity gradient

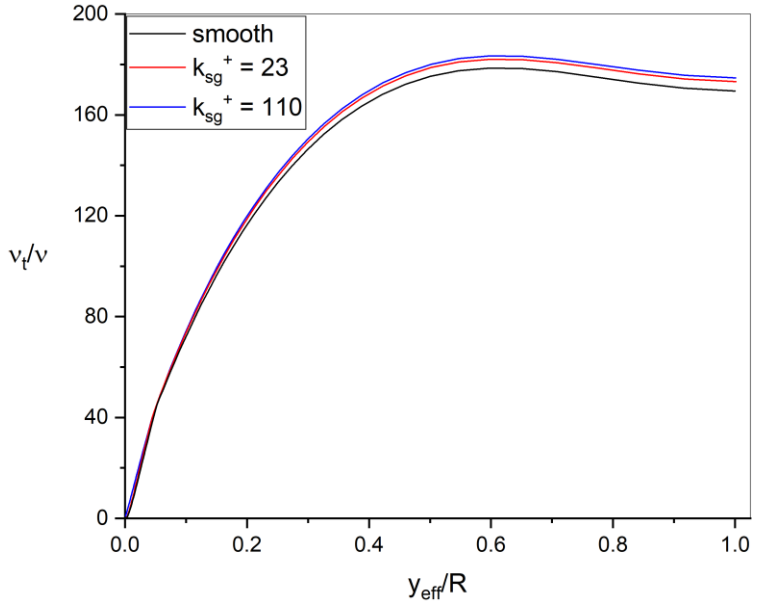

a)

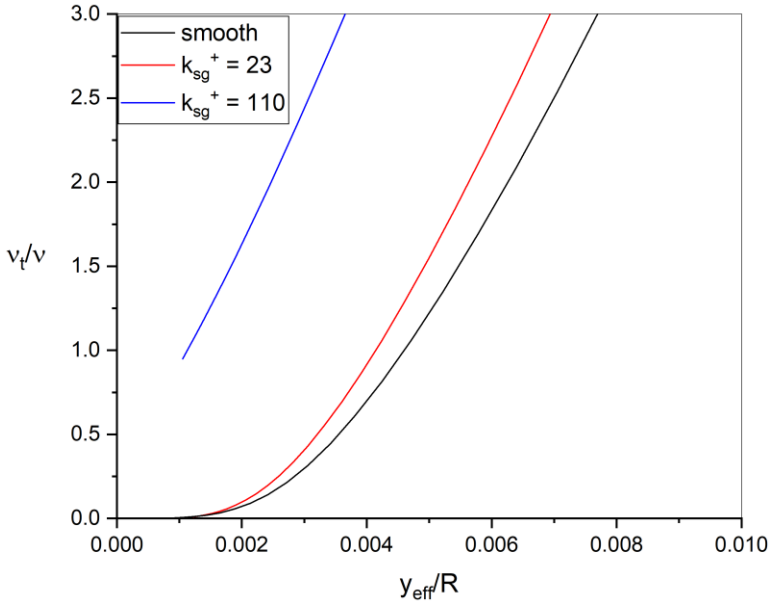

b)

Figure 2.6. a) The profile of normalized eddy viscosity; b) expanded version in the region very close to the wall

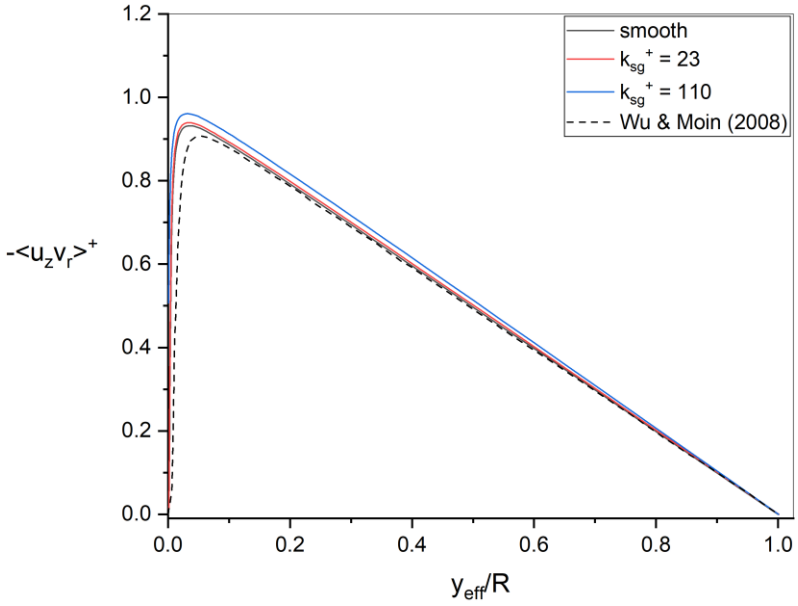

a)

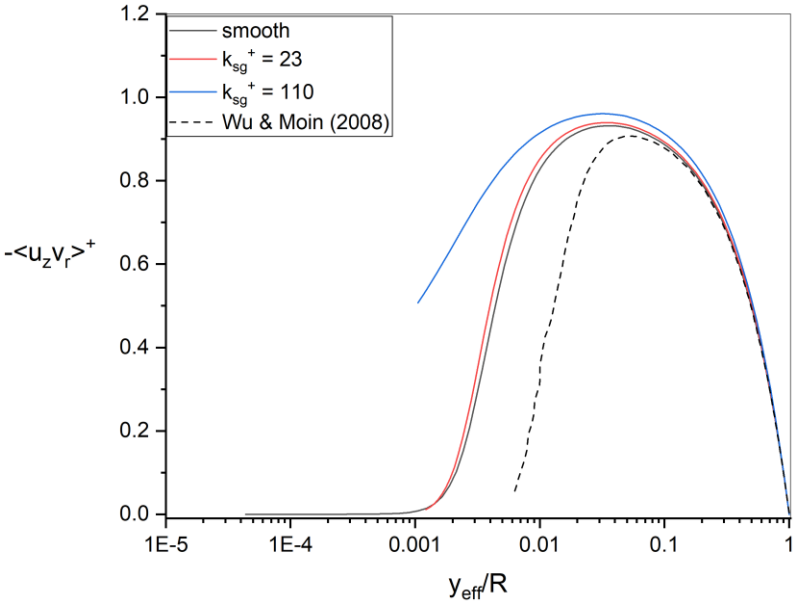

b)

Figure 2.7. a) The profile of normalized Reynolds shear stress on linear scale; b) replot using a logarithmic scale

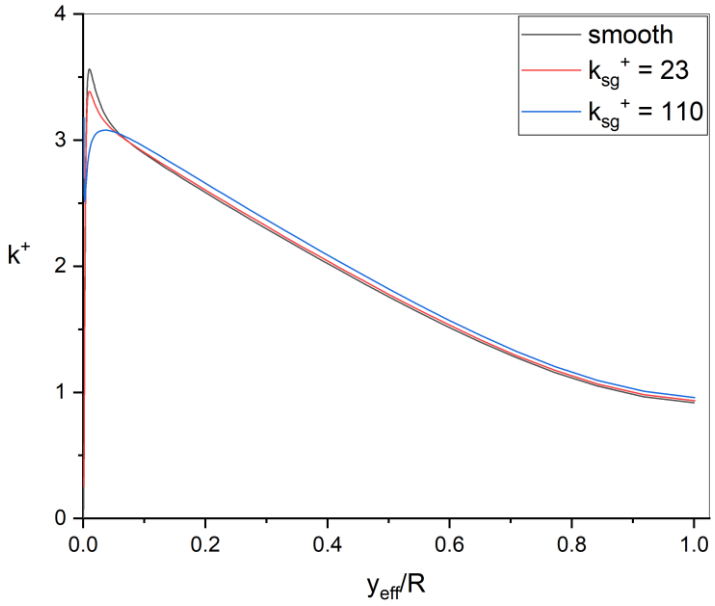

a)

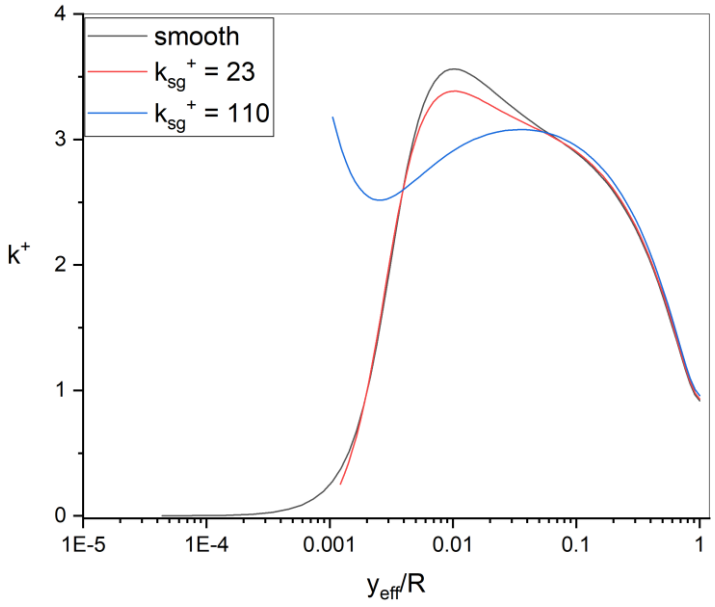

b)

Figure 2.8. a) The profile of normalized turbulence kinetic energy on a linear scale; b) replot using a logarithmic scale

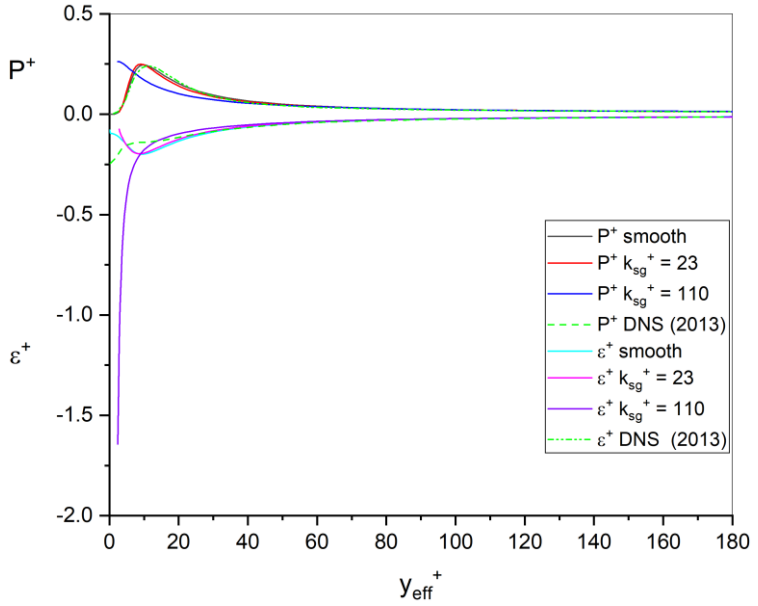

Figure 2.9. The profile of normalized production and viscous dissipation

CHAPTER THREE

PREDICTION OF TURBULENT FLOW OVER A FLAT PLATE WITH A STEP CHANGE FROM A SMOOTH TO A ROUGH SURFACE USING A NEAR-WALL RANS MODEL

Publication:

The manuscript has been submitted as follows:

Chu, M. and Bergstrom, D. J., Prediction of turbulent flow over a flat plate with a step change in roughness from a smooth to a rough surface using a near-wall RANS model, Journal Fluids Engineering, Submitted August 2018

Preamble

The research work presented in this chapter focuses on the second objective of the thesis. More specifically, the performance of the two-layer $k-\varepsilon$ model by Durbin *et al.* (2001) is assessed for the simulation of the turbulent flow over a step change from a smooth to a rough surface, with the special attention to the effects of surface roughness on the mean velocity and turbulence fields downstream of the step. The two-layer model is evaluated by comparing the numerical results to the experimental data in the literature.

Abstract

The present paper reports a numerical study of fully-developed turbulent flow over a flat plate with a step change from a smooth to a rough surface. The Reynolds number based on momentum thickness for the smooth flow was $Re_\theta = 5950$. The focus of the study was to investigate the capability of the Reynolds Averaged Navier Stokes (RANS) equations to predict the internal boundary layer (IBL) created by the flow configuration. The numerical solution used the two-layer $k - \varepsilon$ model of Durbin *et al.* (2001) to implement the effects of surface roughness on the turbulence and mean flow fields via the use of a hydrodynamic roughness length y_0. The prediction for the mean velocity field revealed a transition zone immediately downstream of the step in which the mean velocity profile included a lower region affected by the surface roughness below and an upper region with the characteristics of the smooth-wall boundary layer above. In this zone, both the turbulence kinetic energy and Reynolds shear stress profiles were characterized by a significant reduction in magnitude in the outer region of the flow that is unaffected by the rough surface. The turbulence kinetic energy profile was used to estimate the thickness of the IBL, and the resulting growth rate closely matched the experimental results. As such, the IBL is a promising test case for assessing the ability of RANS models to predict the discrete roughness configurations often encountered in industrial and environmental applications.

Keywords – roughness, internal boundary layer, RANS, two-layer $k - \varepsilon$ model

3.1 Introduction

Turbulent flow has been extensively studied since the turbulent flow regime is so frequently encountered in engineering applications. For example, the design of oil pipelines and aerospace systems require knowledge about the turbulent flow regime. One aspect of turbulence that is challenging both to understand and to model is the interaction of a turbulent flow with a rough surface. Recall that roughness breaks up the viscous sublayer and enhances the local wall shear stress. Presently turbulence models are not able to predict a skin friction distribution based on the surface geometry. Furthermore, most studies of surface roughness have focused on homogeneous distributions of roughness elements, and studied the boundary layers that develop on them. However, in industrial and environmental applications, the surface roughness is often localised and there is a need to better understand these flow scenarios. Flow over a localised patch of surface roughness can begin to be understood using the classical concept of an internal boundary layer.

When a turbulent flow passes over an inhomogeneous surface with a step change in surface roughness, an internal boundary layer (IBL) develops in the region beyond the step. An IBL is frequently encountered in engineering and environmental applications, e.g., icing on the surface of an airfoil, rusting on the interior surface of a pipe, and wind passing from water to land. The descriptor ‘internal’ is adopted since the boundary layer formed over the new surface is within the outer boundary layer upstream of the step. According to Savelyev and Taylor (2005), an internal boundary layer comprises an equilibrium layer in the immediate vicinity next to the wall, and a transition layer with an inflection point in the mean velocity profile. Pendergrass and Arya (1984) had defined the equilibrium layer as the layer in which the turbulent shear stress was in equilibrium with the local surface conditions, and the transition layer as a region in which the flow is undergoing rapid transition from the equilibrium characteristics in the inner layer to that of the outer layer which retains the characteristics of the flow upstream of the step. Within an IBL created by the flow over an abrupt transition from a smooth to a rough surface, the flow in the region next to the wall is influenced by the roughness and the effect of roughness propagates deeper into the outer region as the flow progresses downstream of the step. For the case of flow moving from a smooth to a fully rough surface, the wall shear stress increases abruptly at the step, then decreases, and eventually becomes almost constant with streamwise distance further downstream of the step.

In a pioneering study, Elliott (1958) developed a simple model that can predict the IBL growth downstream from a step change in surface roughness, with a *priori* assumptions of a constant shear stress layer and logarithmic velocity profiles. His model indicated that the IBL grows with distance downstream of the step following a 4/5 power. Panofsky and Townsend (1964) modified Elliott's theory by assuming that the shear stress is a linear function of height. This assumption resulted in the presence of a transition layer that does not appear with Elliott's model. The presence of the transition layer results in a larger height for the IBL compared to that with Elliott's model. The prediction for the growth rate of the IBL is consistent with the prediction by Elliott (1958). Plate and Hidy (1967) developed an analytical model by assuming logarithmic laws for the inner and outer layer of the velocity profile, with a thin transition zone between. The analytical model by Plate and Hidy (1967) gave better overall agreement with the experimental results than the models of Elliott (1958) and Panofsky and Townsend (1964). Referring to published experimental data, Schofield (1981) developed a correlation to approximate the IBL growth after a step change in surface roughness based on a set of relevant parameters. Wood (1981) used dimensional analysis to study the IBL growth after a step change in surface roughness and he developed a general correlation for the height of IBL downstream of the step. All of the above theories concentrated on describing the mean velocity profile and did not consider the turbulent quantities.

Bradley (1968) performed an early atmospheric experiment on the IBL due to a step change in surface roughness for both a smooth-to-rough and rough-to-smooth transition. An abrupt increase in the shear stress at the step was observed in Bradley's experiment. Antonia and Luxton (1971) performed an experimental study of the flow behavior after a smooth-to-rough step change in roughness for a zero pressure gradient boundary layer with the roughness depressed below the smooth surface upstream of the step. They focused on the turbulence structure and growth rate of the IBL and the mean velocity field for the new surface after the step change in roughness. In this paper, a plot of the normalized mean velocity profile as a function of the square root of the wall normal distance was used to locate the inflection point as representative of the height of the IBL. Pendergrass and Arya (1984) conducted an experiment in the EPA Meteorological Wind Tunnel, and observed an abrupt increase in both the shear stress and the turbulent intensity at the step. Cheng and Castro (2002) introduced a different method for determining the thickness of IBL and the equilibrium layer based on the mean velocity profile. They claimed that the thickness of the equilibrium layer varies with the definition. Efros and Krogstad (2011) experimentally studied a

turbulent flow after a step change from a smooth to a rough surface in a closed return wind tunnel. The main purpose of their experiment was to study the effect of the spanwise bar-type roughness on the flow away from the wall in the outer layer, however, their experiment also documents the transition downstream of the step. Meng *et al.* (2016) experimentally studied the IBL behavior in a wind tunnel for a finite section of roughness that created a smooth-to-rough-to-smooth transition in surface conditions.

Unlike previous analytical models of Elliot (1958) and Panofsky and Townsend (1964), Taylor (1968) numerically solved the governing partial differential equations using a mixing length model for the Reynolds shear stress term. However, no discernible change in curvature or inflection point was observed in the velocity profiles predicted by Taylor's (1968) model. Peterson (1968) solved the governing partial differential equations using a turbulence closure based on the hypothesis of Bradshaw *et al*. (1967). The velocity profiles in the transition region predicted by Peterson (1968) did exhibit an inflection point. Peterson's paper reconfirms the 4/5 power law that describes the growth rate of the IBL by previous theories, e.g. Elliott (1958), Panofsky and Townsend (1964), and Taylor (1969). Shir (1971) made improvements over Peterson's theory by including the pressure gradient and equation of motion in the wall-normal direction. Rao (1973) modeled a two-dimensional IBL based on the second moment turbulence model proposed by Lumley and Khajeh-Nouri (1974), which used transport equations for the Reynolds stresses and viscous dissipation rate. Lee and Sung (2007, 2011) used a DNS to analyze the effect of the type of roughness on the IBL downstream of a smooth-to-rough transition. A recent study by Lee (2015) used a DNS to analyze the response of a turbulent flow over a step change from a smooth to a rough surface at a relatively low Reynolds number.

In the present study, the two-layer $k-\varepsilon$ model by Durbin et al. (2001) is used to close the Reynolds Averaged Navier-Stokes (RANS) equations. Presently, RANS models that are able to incorporate the effects of surface roughness are limited. As noted above, an IBL represents a much more complicated turbulent flow configuration than a fully developed turbulent boundary layer over a homogeneous surface. The purpose of this paper is to explore the capability of this RANS model, configured for a rough surface, to predict the effect of a step change from a smooth to a fully rough surface on the mean velocity and turbulence fields.

3.2 The two-layer $k-\varepsilon$ model

3.2.1 Incorporating the effect of roughness

In numerical simulations of turbulent near-wall flow using RANS models, a smooth wall is characterised by the no-slip condition. The mean velocity profile in the overlap region transitions to the wall through a buffer region and the viscous sublayer; the latter is a region where the turbulence is damped and viscous forces are dominant. For a rough surface, the physics is more complicated, since the flow becomes inhomogeneous at the wall due to the variation in surface geometry. For a fully rough wall, the roughness elements completely disrupt the viscous sublayer, and the logarithmic mean velocity profile in the overlap region is observed to extend all the way to the wall. Due to the effective porosity of the wall surface, the turbulence at the wall is non-zero.

In computational models for flows with rough walls, the definition of the wall-normal distance y can be ambiguous. In their two-layer $k-\varepsilon$ model, the y-origin is defined as the location at which the value of mean velocity is extrapolated to zero, e.g. $U(y=0)=0$. For a smooth wall flow, the origin is located right on the wall surface, and the turbulence is also zero at the wall. For a rough wall, this location typically occurs a small distance d below the crest of the roughness elements, as shown in Figure 3.1, and the turbulence is finite at this location. Durbin *et al.* (2001) further introduced the concept of a hydrodynamic roughness length y_o to incorporate the effect of roughness in their two-layer model. More specifically, they defined an effective wall normal distance which was the sum of the wall-normal distance and the roughness length, i.e.

$$y_{\text{eff}} = y + y_0. \tag{3.1}$$

The dimensionless form of y_0 is determined using the calibration curve given in Durbin *et al.* (2001). Figure 3.1 schematically shows the relationship between the y_{eff} and y. When the same wall includes both a smooth region and a rough region, as in the present study, the change in the absolute location of the origin for y between the two regions depends on the physical characteristics of the roughness elements.

Using the concept of hydrodynamic roughness, for fully rough flow the streamwise mean velocity component U in the near-wall region can be defined as follows:

$$U = (u_\tau/\kappa)\ln[(y + y_0)/y_0]. \quad (3.2)$$

In equation (3.2), u_τ is the friction velocity, defined as $(\tau_w/\rho)^{1/2}$, and $\kappa = 0.41$ is von Karman's constant. It is straightforward to show from equation (3.2) that $U = 0$ for $y = 0$. Durbin *et al.* (2001) also noted that based on equation (3.2), the eddy viscosity can be expressed as

$$\nu_t = {u_\tau}^2/(dU/dy) = u_\tau\, \kappa(y + y_0) \quad (3.3)$$

Equation (3.3) indicates that at $y = 0$ the turbulence as measured by the eddy viscosity is finite, and the turbulence itself goes to zero at $y = -y_0$. However, this region is outside the domain of the computation. In this context, Durbin *et al.* (2001) stated that y_o has no physical meaning, but instead is a numerical parameter introduced to incorporate the effect of roughness.

3.2.2 Governing equations

In the present study, the turbulent flow was assumed to be two-dimensional, steady state, isotropic, adiabatic and incompressible. The coordinates x and y represent the streamwise and wall-normal directions, while the symbols U and V represent the mean velocity components in the corresponding directions. The simplified RANS formulation of the continuity and momentum equations is as follows:

$$\frac{\partial U}{\partial x} + \frac{\partial V}{\partial y} = 0. \quad (3.4)$$

$$U\frac{\partial U}{\partial x}+V\frac{\partial U}{\partial y}=g_x-\frac{1}{\rho}\frac{\partial P}{\partial x}+\frac{\partial}{\partial x}\left(\upsilon\frac{\partial U}{\partial x}-<u^2>\right)+\frac{\partial}{\partial y}\left(\upsilon\frac{\partial U}{\partial y}-<uv>\right), \tag{3.5}$$

$$U\frac{\partial V}{\partial x}+V\frac{\partial V}{\partial y}=g_y-\frac{1}{\rho}\frac{\partial P}{\partial y}+\frac{\partial}{\partial x}\left(\upsilon\frac{\partial V}{\partial x}-<uv>\right)+\frac{\partial}{\partial y}\left(\upsilon\frac{\partial V}{\partial y}-<v^2>\right). \tag{3.6}$$

where < > represents time-averaging. The Reynolds stress terms in equations (3.5) and (3.6), i.e. $\langle u^2\rangle, \langle v^2\rangle, \langle uv\rangle$, are unknowns that need to be approximated using a turbulence model.

The two-layer $k-\varepsilon$ model of Durbin *et al.* (2001) combines the high Reynolds number $k-\varepsilon$ model with the $k-l$ model for the region next to the wall. The $k-l$ model abruptly switches to the $k-\varepsilon$ model at a patching point. The transport equations for the turbulence kinetic energy k and its dissipation rate ε in the outer flow are expressed as follows:

k equation

$$\frac{Dk}{Dt}=D_k+P_k-\varepsilon, \tag{3.7}$$

ε equation

$$\frac{D\varepsilon}{Dt}=D_\varepsilon+P_\varepsilon-C_{\varepsilon 2}\frac{\varepsilon}{T}. \tag{3.8}$$

The diffusion and production terms for k and ε in equations (3.7) and (3.8), respectively, are defined as follows:

$$D_k=\frac{\partial}{\partial x}\left[\left(\upsilon+\frac{\upsilon_t}{\sigma_k}\right)\frac{\partial k}{\partial x}\right]+\frac{\partial}{\partial y}\left[\left(\upsilon+\frac{\upsilon_t}{\sigma_k}\right)\frac{\partial k}{\partial y}\right], \tag{3.9}$$

$$P_k = -<u^2>\frac{\partial U}{\partial x} - <v^2>\frac{\partial V}{\partial y} - <uv>\frac{\partial U}{\partial y} - <uv>\frac{\partial V}{\partial x}, \quad (3.10)$$

$$D_\varepsilon = \frac{\partial}{\partial x}\left[\left(\upsilon + \frac{\upsilon_t}{\sigma_\varepsilon}\right)\frac{\partial \varepsilon}{\partial x}\right] + \frac{\partial}{\partial y}\left[\left(\upsilon + \frac{\upsilon_t}{\sigma_\varepsilon}\right)\frac{\partial \varepsilon}{\partial y}\right], \quad (3.11)$$

$$P_\varepsilon = C_{\varepsilon 1} P_k / T, \quad (3.12)$$

where the turbulent time-scale is given by $T = k/\varepsilon$. In addition, v and ν_t are the molecular and turbulent kinematic viscosity, respectively, with the model constants $\sigma_k = 1.00$ $\sigma_\varepsilon = 1.30$, $C_{\varepsilon 1} = 1.44$ and $C_{\varepsilon 2} = 1.92$ following Durbin *et al*. (2001).

The Reynolds stress terms were approximated by a Boussinesq eddy viscosity model. Using this model, the shear stress terms are written as follows:

$$-<uv> = \nu_t\left(\frac{\partial U}{\partial y} + \frac{\partial V}{\partial x}\right). \quad (3.13)$$

In Equation (3.13), ν_t has dimensions such that it can be represented by the product of a turbulent velocity scale v [m/s] and a turbulent length scale l [m]. Then, ν_t can be expressed as follows:

$$\nu_\mathrm{t} = C_\nu v l, \quad (3.14)$$

where $C_\mathrm{v} = 0.09$ is a dimensionless constant, and v and l are related to k and ε as follows:

$$v = k^{1/2}, \quad (3.15)$$

$$l = k^{3/2}/\varepsilon. \quad (3.16)$$

Therefore, for the classical $k-\varepsilon$ model, ν_t is specified by

$$\nu_t = C_\nu k^2/\varepsilon. \tag{3.17}$$

The $k-l$ model incorporates the effect of the wall on ν_t and ε into equations (3.14) and (3.16) as follows:

$$\upsilon_{\mathrm{t}} = C_\nu \sqrt{k} l_\nu, \tag{3.18}$$

$$\varepsilon = k^{3/2}/l_\varepsilon, \tag{3.19}$$

where l_ν and l_ε are length scales governed by a Van Driest damping function, written as follows:

$$l_\varepsilon = C_l y_{\mathrm{eff}}(1 - e^{-R_{y/A_\varepsilon}}), \tag{3.20}$$

$$l_\upsilon = C_l y_{\mathrm{eff}}(1 - e^{-R_{y/A_\nu}}), \tag{3.21}$$

where $C_l = 2.5$, $A_\varepsilon = 2C_l = 5.0$, A_ν is a constant (depends on flow regimes) and $R_y = y_{\mathrm{eff}}\sqrt{k}/\nu$ is the wall-distance Reynolds number. In the region next to the wall, the flow behavior is described by the $k-l$ model, and at the patching point, characterized as $1 - e^{-R_y/A_\nu} = 0.95$, the $k-\varepsilon$ model is employed to describe the flow behavior in the region away from the wall. This condition holds true for both smooth and rough flow cases. The value of the coefficient A_ν is adjusted for a rough wall to reduce the wall damping. Durbin *et al*. (2001) used the following linear interpolation:

$$A_\nu = max\left[1, A_\nu^0(1 - k_{\mathrm{sg}}^+/90)\right]. \tag{3.22}$$

for a surface characterised in terms of equivalent sand grain roughness k_{sg}. $A_\nu = A_\nu^0 = 62.5$ for smooth flows. In equation (3.22), the subscript $(\,)^+$ denotes a quantity non-dimensionalized with the viscous length scale given by ν/u_τ, where u_τ is the friction velocity. Note that for fully rough conditions, $A_\nu = 1$, and $1 - e^{-R_y/A_\nu}$ is very close to unity, so that l_ν becomes $C_l y_{\text{eff}}$, implying very little damping effect on the flow.

For a smooth wall, the boundary condition for k is $k(y = 0) = 0$. For a rough wall flow, the boundary condition for k is a quadratic interpolation given by

$$k(y = 0) = u_\tau^2/\sqrt{C_\nu}\, min\left[1, (k_{sg}^+/90)^2\right], \tag{3.23}$$

Irrespective of roughness, the boundary condition for ε is given by

$$\varepsilon(y = 0) = \nu k(0) A_\varepsilon / y_0^2 C_l. \tag{3.24}$$

Equation (3.23) and (3.24) indicate that k and ε are finite at $y = 0$ for a rough wall.

3.2.3 Flow description and numerical method

The flow being considered is over a flat plate (zero pressure gradient) with a step-change in roughness, as shown in Figure 3.2. Beyond the step, an IBL (δ_i) develops in the streamwise direction within the outer boundary layer (δ). The solution domain is two-dimensional and uses a Cartesian coordinate system. It is $L =$ 4.0 m long and $H = 0.2$ m high in the streamwise (x) and wall-normal (y) directions, respectively. The domain height of 0.2 m ensures that the domain is twice the height of the boundary layer thickness at the end of the plate. The bottom plate comprises a smooth and a rough surface, with a 2 m distance for each surface. The step change from a smooth to a rough surface is located at the midpoint of the plate, which is similar to the experimental arrangement used by Antonia and Luxton (1971).

The present study used a uniform grid of 273 control volumes in the streamwise direction, and a non-uniform grid of 140 control volumes in the wall-normal direction, which are concentrated near the bottom wall. For comparison, in their simulation of flow over an airfoil, Im and Zha (2014) also used a uniform grid in the streamwise direction. Their fine mesh control volume size was $\Delta x = 0.0042L$, where L is the length of the plate. For the present study, $\Delta x = 1.47 \times (10)^{-2}$m, which corresponds to $\Delta x \cong 0.0037L$, which is comparable to their value. The first grid node in the wall-normal direction was placed at a distance of $y = 1.07 \times (10)^{-6}$m above the wall, which corresponds to $y^+ = 0.18$ at $x/L = 0.49$. Further refining the grid did not result in significant changes to the solution field.

The fluid was assumed to be air, with a density of $\rho = 1.2$ kg/m^3 and kinematic viscosity of $\nu = 1.5 \times 10^{-5}$ m^2/s. For the smooth wall, the boundary condition for the mean velocity assumed a no-slip condition. An equivalent sand-grain roughness value of $k_{sg}^+ = 110$ was specified for the rough surface to ensure a fully rough velocity profile. At the inlet of the domain, the freestream velocity was set equal to 30 m/s, which corresponds to a Reynolds number based on the plate length of $Re = 3.94 \times 10^6$. At the top of the domain, zero velocity gradient was specified for U and V ($\partial / \partial \mathrm{y} = 0$). At the outlet of the domain, flow was assumed to be at a fully-developed state. The boundary conditions at the wall for k and ε were given in the previous section.

In the present study, nine locations were selected downstream of the step to evaluate the flow development in the streamwise direction, i.e. $x_1 = x/L = 0.51$, $x_2 = x/L = 0.52$, $x_3 = x/L = 0.53$, $x_4 = x/L = 0.55$, $x_5 = x/L = 0.60$, $x_6 = x/L = 0.65$, $x_7 = x/L = 0.70$, $x_8 = x/L = 0.79$, and $x_9 = x/L = 0.85$. The smooth-wall velocity profile at x_s was sufficiently close to the step to be used as a reference for the rough-wall velocity profiles downstream of the step.

The numerical solution used an in-house Fortran code instead of commercial software to enable complete control over the wall treatment required by the two-layer $k - \varepsilon$ model. The transport equations were discretized on a staggered mesh using the finite volume method. The differencing scheme used a power law relation to approximate an exponential differencing scheme. The set of linear coupled algebraic equations was solved using a segregated solution technique, and the pressure solver followed the SIMPLEC algorithm. The solution fields were iterated until convergence, which typically required approximately 1300 iterations. The normalized residual for

mass conservation was approximately $\sim 10^{-6}$, while the residuals of momentum, turbulence kinetic energy and dissipation rate equations were approximately $\sim 10^{-5}$.

3.3 Results and discussion

3.3.1 Skin friction coefficient

Perhaps the most important parameter for a boundary layer is the local wall shear stress, which in dimensionless form becomes the skin friction coefficient. Figure 3.3 shows the prediction for the skin friction coefficient $c_f = 2(u_\tau/U^2)$ as a function of the dimensionless streamwise distance x/L. In Figure 3.3, the predicted c_f is plotted using discrete points to highlight the value of c_f for each control volume. Empirical correlations for c_f by Schultz-Grunov (1979) and Schlichting (1979) for a smooth and rough surface, respectively, are included for comparison. For the smooth-wall flow, there is good agreement between the predicted value of c_f and the correlation by Schultz-Grunov (1979), with a peak value of approximately $c_f = 0.01$ at the leading edge. The predicted decay for the value of c_f over the smooth surface is well captured by the two-layer model.

At the initial location of the roughness, i.e. $x/L \sim 0.5$, the prediction for c_f jumps to a value which is significantly larger than the fully-developed value for the rough surface. Furthermore, before c_f reaches the peak value downstream of the step, jumps in the value of c_f can be observed immediately ahead of the step change in surface condition. Abrupt increase in the value of c_f around a step change in surface roughness has been observed by previous studies, e.g. Bradley (1968), Pendergrass and Arya (1984), and Lee (2015). Downstream of the peak, the value of c_f begins to smoothly decrease and approaches a nearly constant value near the end of the plate. Smalley *et al.* (2001) proposed that the value of c_f should remain relatively constant along the streamwise direction when the flow reaches self-preservation conditions. For the rough wall region downstream of the peak, the correlation by Schlichting (1979) sits just slightly above the predicted c_f profile, showing overall good agreement between the prediction and the correlation.

3.3.2 Evaluating the height of the IBL

Different methods have been developed to determine the IBL thickness. Efros and Krogstad (2011) used the method proposed by Krogstad and Nickels (2006) to locate the IBL thickness by fitting two straight lines to the distribution of the streamwise normal Reynolds stress throughout the entire BL. In this paper, the method of Krogstad and Nickels (2006) is adopted, but applied to the profile of the turbulence kinetic energy. In Figure 3.4, the OriginLab software was used to fit two straight lines (in red) to the predictions for the normalized turbulence kinetic energy k^+ for $x/L = 0.51$, and the intersection of these two lines is taken as the height of IBL, δ_i , which is where the IBL merges with the outer BL. For comparison, the height of the IBL, denoted δ_{ip} , at the same location was also approximated using the inflection point method of Antonia and Luxton (1971) as shown in Figure 3.5. At the location $x_1 = 0.51L$, the values of $\delta_i = 4.61$ mm and $\delta_{ip} = 3.13$ mm were within approximately 30 percent of each other. Both methods require some judgment regarding the fitting of the straight line segments, which introduces an uncertainty in the calculation.

Figure 3.6 shows the predicted results taken at various locations downstream of the step tracing the development of the IBL using the two different methods. From Figure 3.6, δ_i and δ_{ip} increase as the flow develops downstream from the step, with δ_i laying somewhat above δ_i. With the inflection point method, the intersection between the edge of IBL and the outer BL becomes less apparent further downstream of the step. This results in the last point missing for the prediction of δ_{ip} as compared to δ_i, as shown in Figure 3.6. The discrepancy is smaller in the immediate vicinity of the step and gradually increases as the flow proceeds further in the streamwise direction. Savelyev and Taylor (2005) proposed that the inflection point is strictly within the transition layer, which is somewhat below the outer edge of the IBL. This might partly explain the differences between the two methods observed in Figure 3.6. Power laws are fitted to the predicted results for δ_i and δ_{ip}, depicted by the red dashed line and green dotted line, respectively. Based on the results plotted in Figure 3.6, the predictions for δ_i increase at a rate proportional to $x^{0.73}$, which agrees well with the conclusion of Antonia and Luxton (1971), $\delta_{ip} \sim x^{0.72}$.

Figure 3.7 shows the streamwise development of the IBL and BL downstream of the step using δ_i and δ, respectively. The intersection of the two dashed straight lines, i.e. $x/L = 0.72$, as shown in Figure 3.7, is the approximate location where the transition zone ends and the equilibrium zone

starts. From Figure 3.7, δ_i increases quickly in the transition zone to merge with δ for $x/L \cong 0.72$. Beyond $x/L \cong 0.72$, the flow enters the equilibrium zone, where the internal boundary layer and outer boundary layer have merged. Thereafter, the flow above the plate is in equilibrium with the new surface conditions, i.e. the roughness. Using the method shown in Figure 3.4, the intersection point becomes less pronounced as the flow proceeds further downstream from the step. This phenomenon was also observed by Antonia and Luxton (1971), i.e. the 'knee' point became less apparent as the flow develops downstream of the step. The above analysis implies that it is difficult to precisely predict the location at which δ_i merges with δ.

3.3.3 Streamwise mean velocity

Predictions for the mean streamwise velocity component (U) profiles as a function of the dimensionless wall-normal distance y_{eff}/δ are shown Figure 3.8a) and b) for the transition zone and the equilibrium zone. The structure of this plot is suggested by Figure 4 in the early and seminal study of Rao *et al.* (1974). The smooth-wall velocity profile for U at x_s is included as a reference value. Note that all of the rough-wall velocity profiles are plotted to begin at the location where the mean velocity is zero, i.e. where $y_{\text{eff}} = y_0$. The smooth-wall velocity profile is plotted beginning at the first node above the wall, where the velocity is finite. It is clear that the smooth-wall velocity profile retains a viscous sublayer, which is absent in the case of the rough-wall velocity profiles. The physical location of the origin of the rough profiles relative to the smooth surface is not specified and depends on the characteristics of the roughness elements. Finally note that the use of a logarithmic scale on the ordinate axis greatly expands the region very close to the wall.

The U profiles across the entire boundary layer are plotted in Figure 3.8a). From Figure 3.8a), the rough-wall velocity profiles deviate from the smooth-wall velocity profile due to the increase in wall shear stress, and hence the value of c_f, on the rough surface. Outside the roughness sublayer the effect of the enhanced wall shear stress in reducing the momentum is greatest near the step and decreases downstream. The decrease in momentum propagates higher into the boundary layer as the flow proceeds downstream of the step. At the outer edge of the boundary layer where $y_{eff}/\delta = 1$, all of the velocity profiles recover to the freestream value. A conclusion to be drawn from Figure

3.8a) is the further the flow travels downstream from the step, the deeper the effect of roughness propagates into the outer boundary layer. However, within the transition zone the upper portion of the outer boundary layer retains the characteristics of the smooth-wall flow upstream of the step, and as such is not in equilibrium with the rough-surface below. Figure 8a) exhibit a distinct change in curvature indicated by an inflection point. The open circles in Figure 3.8a) indicate the approximate thickness of the IBL using the method of Antonia and Luxton (1971) for the velocity profiles over the rough surface.

Figure 3.8b) present the predictions for the streamwise velocity profiles on the rough surface for the equilibrium zone. In the equilibrium zone, the velocity profiles become almost indistinguishable from each other, indicating a type of similarity. This indicates that the effect of roughness has now permeated the entire outer boundary layer, and the flow becomes insensitive to the surface conditions upstream of the step. There are no inflection points in the U profiles in the equilibrium zone.

3.3.4 Mean streamwise velocity using inner coordinates

The mean streamwise velocity profiles at different sections are shown in Figure 3.9a) and b), where U^+ and y^+_{eff} are the mean streamwise velocity and effective wall-normal distance normalized using inner coordinates, i.e. $U^+ = U/u_\tau$ and $y^+_{\text{eff}} = yu_\tau/\nu$, respectively, where u_τ is the local friction velocity. Also included are the canonical logarithmic velocity profile for a smooth and fully rough surface, as well as the smooth wall direct numerical simulation (DNS) data of Schlatter *et al.* (2011) for a turbulent boundary layer on a smooth surface with a Reynolds number based on momentum thickness of $Re_\theta = 4100$. Figure 3.9a) shows that the predicted smooth-wall U^+ profile agrees well with both the DNS data and the canonical logarithmic profile in the overlap region for $30 < y^+_{\text{eff}} < 500$. In the present study, $y^+_{\text{eff}} = 500$ corresponds to the $y_{\text{eff}}/\delta = 0.15$ (inner region). Note that both the DNS profile and velocity profile predicted by the two-layer model exhibit a strong wake component near the outer edge of the boundary layer; the wake is strongest for the DNS profile. The increase in u_τ due to roughness ($k^+_{\text{sg}} = 110$) results in a downward shift of approximately $\Delta U^+ \cong 8.20$ in the predicted rough-wall U^+profiles compared to the smooth U^+ profile, as shown in Figure 3.9a). This is close to the downward shift of $\Delta U^+ = 7.99$ given by the

Prandtl-Schlichting relation. With this downward shift, all of the predicted rough-wall velocity profiles collapse onto a single curve for the overlap region; however, they deviate from each other in the outer region. A similar behavior was observed by Efros and Krogstad (2011) in their experimental study. In addition, the predicted rough U^+ profiles remain almost logarithmic up to the wall. This indicates the fact that viscous sublayer is completely disrupted by the roughness, and the viscous transport becomes insignificant close to the wall.

Figure 3.9b) enlarges the outer region of the boundary layer to highlight the flow behavior for $y_{\text{eff}}^+ > 100$. In this region, Figure 3.9b) clearly shows that the predicted rough-wall U^+ profiles for positions further downstream from the step tend to approach closer to the logarithmic profile. This is due to the propagation of the effect of roughness deeper into the outer boundary layer as the flow develops in the streamwise direction downstream from the step. This behavior was also observed by Efros and Krogstad (2011). At the outer edge of the boundary layer, the different values of U_e^+ for the rough-wall profiles, as shown in Figure 3.9b), is due to the gradual decrease in the value of c_f and hence u_τ along the rough surface.

3.3.5 Mean defect velocity profile

The predictions for the mean defect velocity profile normalized by u_τ, i.e. $(U_e - U)/u_\tau$, are presented in Figure 3.10. The experimental data of Efros and Krogstad (2011), for a much higher Reynolds number flow ($Re_\theta = 1.3 \times 10^4 - 3.2 \times 10^4$) and a much larger equivalent sandgrain roughness ($k_{\text{sg}}^+ \sim 10^3$), is included for comparison. In Figure 3.10, x' is the distance measured from the step, where $x' = 0$ at the step. In the experiment of Efros and Krogstad (2011), $x' = 0$ for the smooth-wall flow, $x' = 200$ and 700 mm for the transition zone, and $x' = 2200$ mm for the equilibrium zone. For the smooth-wall flow, Figure 3.10 shows that the predicted profile agrees well with the experimental data for the inner region of $y_{\text{eff}}/\delta < 0.2$, and sits slightly below the experimental data for the region of $y_{\text{eff}}/\delta > 0.2$. Figure 3.10 shows that the predictions and experimental data are similar in shape for the transition zone: the concavity of the profile strongly increases after the step, and then relaxes as the flow moves further downstream. For the equilibrium zone, the predicted rough-wall profile at x_8 now nearly collapses onto the predicted smooth-wall profile, with a small discrepancy in the outer region for $y_{\text{eff}}/\delta > 0.2$. Recall that

turbulent boundary layer theory suggests that a smooth and fully rough velocity profile share the same dimensionless defect profile outside the roughness sublayer, which is consistent with the behavior shown in Figure 3.10. This behavior can also be observed in the experimental measurements of Efros and Krogstad (2011), and the DNS data of Lee and Sung (2007).

3.3.6 Reynolds shear stress profiles

The predicted profiles for the Reynolds shear stress normalized with the friction velocity squared, $-< uv >^+$ are shown in Figure 3.11a) and b). Figure 11b) expands the near-wall region by using a logarithmic scale for y_{eff}/δ. The experimental data of Efros and Krogstad (2011) for a similar flow is included for comparison, as well as the boundary layer measurements of Flack *et al.* (2007) ($Re_\theta = 7.3 \times 10^3 - 13 \times 10^3$) and Krogstad and Antonia (1999) ($Re_\theta = 12800$), as well as the DNS data of Lee and Sung (2011) ($Re_\theta = 1300$). In Figure 3.11a), the prediction for the smooth-wall $-< uv >^+$ profile shows good agreement with the results of Efros and Krogstad (2011) for $y_{\text{eff}}/\delta > 0.2$. For the smooth-wall flow, the present prediction also matches the DNS profile of Lee and Sung (2011) except in the region $y_{\text{eff}}/\delta < 0.2$, where it gives a larger value of $-< uv >^+$. This discrepancy is due to the fact that the value of Re_θ for the prediction is four-times larger than that for the DNS data, i.e. $Re_\theta \cong 5950$ compared to $Re_\theta \cong 1300$. The predicted $-< uv >^+$ profile peaks around the value of 0.95 for the smooth wall flow, which is slightly larger than the peak value of 0.90 obtained by Lee and Sung (2011). According to Degraaff and Eaton (2000) and Marusic and Kunkel (2003), the peak value of the Reynolds shear stress for smooth flows tend to increase with Reynolds number.

For the transition zone, the predictions for the rough-wall $-< uv >^+$profiles at x_4 and x_6 show the same effect as the experimental data of Efros and Krogstad (2011) for $x' = 200$ and 700 mm, i.e. a strong reduction of the Reynolds stress profile in the outer region of the flow. The magnitude of the reduction is much greater for the experimental data due to the larger roughness elements used in that study. For the predicted fields the reduction is greatest close to the step, i.e. x_4 and the second profile at x_6 begins to recover toward the equilibrium profile.

For the equilibrium zone, the prediction for the $-< uv >^+$ profile in general shows good agreement with the experimental data of Efros and Krogstad (2011) for $x' = 4800$ mm, although

the discrepancy becomes larger in the far outer region, i.e. $y_{\text{eff}}/\delta > 0.7$. On the other hand, the prediction shows good agreement with the experimental data of Krogstad and Antonia (1999) for the inner region $y_{\text{eff}}/\delta < 0.3$, and begins to gradually deviate for $y_{\text{eff}}/\delta > 0.3$. As expected, the predicted peak value for $-< uv >^+$ is approximately one for both the transition and the equilibrium zone, which agrees well with the experimental studies. From Figure 3.11a), the predicted rough-wall $-< uv >^+$ profile for the equilibrium zone is consistently greater than the predicted smooth-wall profile, and the difference extends almost to the outer edge of the boundary layer. However, the magnitude of the difference is relatively small, and similar behavior has been observed by other researchers as well, e.g. Efros and Krogstad (2011) and Krogstad and Antonia (1999).

Figure 3.11b) uses a logarithmic scale for y_{eff}/δ to highlight the values very close to the wall. The prediction for the smooth-wall $-< uv >^+$ profile lies slightly above the experimental data of Flack *et al.* (2007), but overall shows good agreement with that data set in the inner region. From Figure 3.11b), the prediction for the smooth-wall profile reduces to zero as the wall is approached. On the other hand, all of the predicted rough-wall profiles retain a finite value of approximately $-< uv >^+ \cong 0.5$ at the first grid above the wall. Figure 3.11b) clearly shows that within the inner region of $y_{\text{eff}}/\delta < 0.2$ the predictions for the rough-wall $-< uv >^+$ profiles sit much higher than the prediction for the smooth $-< uv >^+$ profile, indicating that strong turbulence is present very close to the rough surface.

3.3.7 Turbulence kinetic energy profile

The profiles predicted for the turbulence kinetic energy normalized by the friction velocity squared, k^+, are shown in Figure 3.12 a) and b), and the experimental measurements of Krogstad and Antonia (2001) and Erm (1988) ($Re_\theta = 2788$) are included for comparison. As before, Figure 3.12b) expands the region in the immediate vicinity of the wall by using a logarithmic scale for y_{eff}/δ. In general the prediction for the smooth-wall k^+ profile shows good agreement with the experimental data of Erm (1988). Beyond the region of $y_{\text{eff}}/\delta > 0.6$, the predicted smooth-wall k^+ profile lies somewhat above the experimental data of Erm (1988), while near the wall the predicted peak value is both smaller and located much closer to the wall.

For the transition zone, the predicted rough-wall k^+ profiles are significantly reduced in magnitude compared to the smooth-wall case. The reduction is greatest closer to the step and thereafter the profile begins to recover toward the equilibrium value. This behaviour was also observed for the Reynolds shear stress profile. For the equilibrium zone, the predicted rough-wall k^+ profile lies slightly above that for the smooth wall in the outer flow, $y_{\text{eff}}/\delta > 0.1$. On the other hand, the predicted rough-wall k^+ profile for the equilibrium zone lies significantly below the experimental data of Krogstad and Antonia (2001) for the region of $y_{\text{eff}}/\delta < 0.7$.

Figure 3.12b) expands the region next to the wall using the logarithmic scale on y_{eff}/δ to focus on the values in the vicinity of the wall. From Figure 3.12b), the prediction for the smooth k^+ profile reduces to zero as the wall is approached. After the flow encounters the step change in surface roughness, the predictions for the rough-wall k^+ profiles retain a finite value of approximately $k^+ \cong 3.1$ at the first control volume above the wall, which represents a second near-wall peak for the rough-wall k^+ profiles. From Figure 3.12 a) and b), it can be observed that these two peaks in the rough-wall k^+ profiles have approximately the same magnitude. In general, the predictions for the rough-wall k^+ profiles lie significantly above the smooth-wall profile in the immediate vicinity of the wall, i.e. $y_{\text{eff}}/\delta < 0.004$. This indicates a much stronger turbulence kinetic energy than that for the smooth surface is produced in the region very close to the wall for the rough surface.

3.4 Conclusions

Steady, incompressible turbulent flow over a step change from a smooth to a fully rough surface at $Re_\theta = 5950$ has been investigated using a two-layer $k-\varepsilon$ model configured for including the effects of surface roughness. The predictions for the skin friction coefficient for the smooth and the rough surfaces were in good agreement with the correlations of Schultz-Grunov (1979) and Schlichting (1979), respectively. The predicted skin friction coefficient sharply increases at the step and then quickly relaxes to a level characteristic of fully rough flow.

The flow downstream of the step can be characterized by a transition zone in which the mean velocity profile shows a change in curvature or inflection point. The inflection point was displaced higher as the flow moved further downstream of the step, which was interpreted as the transverse propagation of the effects of the rough surface into the outer smooth-wall boundary layer. At the

end of the transition zone, the entire velocity profile was in equilibrium with the rough surface below. A new method based on the characteristic shape of the turbulence kinetic energy profile in the transition zone was used to estimate the thickness of the IBL. The predicted thickness of the IBL increased at a rate proportional to $x^{0.73}$, which is in a good agreement with the experimental result of $x^{0.72}$ measured by Antonia and Luxton (1971).

When the predictions for the mean velocity profile were plotted in inner coordinates on a log-law plot, the lower section of the velocity profiles in the transition zone closely matched the straight-line curve for a fully rough velocity profile, with a downward shift of $\Delta U^+ \sim 8.20$. The prediction for the mean velocity field was also analyzed using the mean defect law. In the transition zone, the mean defect profile $U_e^+ - U^+$ initially collapsed to sit well below the smooth-wall profile, before recovering downstream to a fully-rough profile that was very close to the smooth-wall result. This behaviour is qualitatively very close to that observed by Efros and Krogstad (2011).

The dimensionless Reynolds shear stress $-< uv >^+$ and turbulence kinetic energy k^+ profiles were also analyzed. The smooth-wall profiles were close to experimental results extracted from the literature. Likewise, at the end of the transition zone, the equilibrium profiles compared favorably with the profiles for fully-rough flows documented in the literature. In the transition zone, the profile for both quantities showed a collapse and recovery cycle that was similar to that of the mean defect profile. For the dimensionless Reynolds shear stress profiles, the behaviour was very similar to that documented in the experimental study of Efros & Krogstad (2011).

One of the special features of the two-layer model is the ability to predict the flow very close to the wall. For the rough wall, both the dimensionless Reynolds stress and turbulence kinetic energy profiles behaved much differently than for the smooth-wall case. For a smooth wall, both properties reduce to zero, for the fully rough case, both profiles retain finite values at the wall. Unfortunately, there are no experimental data available for evaluating the predictions for the turbulence properties within the roughness elements where the mean velocity reduces to zero.

Overall, the two-layer model was very effective in reproducing the characteristics of an IBL created by a step change from a smooth to a rough surface on a flat plate. Future work will focus on understanding better the flow immediately downstream of the step, where the surface condition first begins to interact with the incoming boundary layer.

3.5 References

Antonia, R. A. and Krogstad, P.-A., 2001. Turbulence structure in boundary layers over different types of surface roughness. *Fluid Dynamics Research*, Vol. 28, pp. 139-157.

Antonia, R. A. and Luxton, R. E., 1971. The response of a turbulent boundary layer to a step change in surface roughness Part1. Smooth to rough. *Journal of Fluid Mechanics*., Vol. 48, pp. 721-761.

Bradley, E. F., 1968. A micrometeorological study of velocity profiles and surface drag in the region modified by a change in surface roughness. *Journal of the Royal Meteorological Society*, Vol. 94, pp. 361-379.

Bradshaw, P., Ferriss, D.H., and Atwell, N.P., 1967. Calculation of boundary-layer development using the turbulent energy equation. *Journal of Fluid Mech*., Vol. 28, pp. 593-616.

Cheng, H. and Castro, I. P., 2002. Near-wall flow development after a step change in surface roughness. *Boundary-Layer Meteorology*, Vol. 105, pp. 411-432.

Degraaff, D. B., and Eaton, J. K., 2000. Reynolds-number scaling of the flat-plate turbulent boundary layer. *Journal of Fluid Mechanics*, Vol.422, pp.319-346.

Durbin, P. A., Medic, G., Seo, J.-M, Eaton, J. K., and Song, S., 2001. Rough wall modification of two-layer k-ε model. *Journal of Fluids Engineering*, Vol. 123, pp. 16-21.

Elliott, W. P., 1958. The growth of the atmospheric internal boundary layer. *American Geophysical Union.* Vol. 39, pp.1048-1054.

Erm, L., 1988. Low-Reynolds-Number Turbulent Boundary Layers. *PhD Thesis*, University of Melbourne.

Flack, K. A., Schultz, M. P., and Connelly, J. S., 2007. Examination of a critical roughness height for outer layer similarity. *Physics of Fluids*, Vol. 19, pp.1-9.

Im, H.-S., and Zha G.-C., 2014. Delayed detached eddy simulation of airfoil stall flows using high-order schemes. *Journal of Fluids Engineering*, Vol. 136, pp. 1-12.

Krogstad, P.-A., and Antonia, R. A., 1999. Surface roughness effects in turbulent boundary layers. *Experiments in Fluids*, Vol. 27, pp. 450-460.

Krogstad, P.-A and Efros, V., 2011. Development of a turbulent boundary layer after a step from smooth to rough surface. *Experiments in Fluids*, Vol. 51, pp. 1563-1575.

Krogstad P.-A., and Nickels T., 2006. Turbulent boundary layer with a step change in surface roughness. *Conference on modelling fluid flow (CMFF'06)*, Budapest, Hungary.

Lee, S.-H., and Sung H. J., 2007. Direct numerical simulation of the turbulent boundary layer over a rod-roughened wall. *Journal of Fluid Mechanics.*, Vol. 584, pp. 125-146.

Lee, J. H., Sung, H. J. and Krogstad, P.-A., 2011. Direct numerical simulation of the turbulent boundary layer on a cube-roughened wall. *Journal of Fluid Mechanics*., Vol. 669, pp. 397-431.

Lee, J. H., 2015. Turbulent boundary layer flow with a step change from smooth to rough. *International Journal of Heat and Fluid Flow*, Vol. 54, pp. 39-54.

Lumley, J. L. and Khajeh-Nouri, B., 1974. Computational modeling of turbulent transport. *Advances in Geophysics*, Vol. 18, pp. 169-192.

Marusic, I., and Kunkel, G.J., 2003. Streamwise turbulence intensity formulation for flat-plate boundary layers. *Physics of Fluids*, Vol. 15, pp. 2461-2464.

Meng F., Bergstrom D. J., and Wang BC., 2016. Scaling the internal boundary layer. In: Stanislas M., Jimenez J., Marusic I. (eds) Progress in wall turbulence 2. ERCOFTAC Series, Vol. 23. Springer, Cham.

Panofsky, H. A. and Townsend A. A., 1964. Change of terrain roughness and the wind profile. *Journal of the Royal Meteorological Society*, Vol. 90, pp. 147-155.

Peterson, E. W., 1969. Modification of mean flow and turbulent energy by a change in surface roughness under conditions of neutral stability. *Journal of the Royal Meteorological Society*, Vol. 95, pp. 561-575.

Pendergrass, W. and Arya S.P.S., 1984. Dispersion in neutral boundary layer over a step change in surface roughness – 1. Mean flow and turbulence structure. *Atmospheric Environment*, Vol. 18, pp. 1267-1279.

Plate, E. J. and Hidy G. M., 1967. Laboratory study of air flowing over a smooth surface onto small water waves. *Journal of Geophysical Research*, Vol. 72, pp.4627-4641.

Rao, K.S., Wyngaard, J.C., and Cote, O.R., 1973. The structure of the two-dimensional internal boundary layer over a sudden change of surface roughness. *Journal of the Atmospheric Sciences*, Vol. 31, pp. 738-746.

Savelyev, S.A. and Taylor, P.A., 2005. Internal boundary layers: 1. Height formulae for neutral and diabatic flows. *Boundary-Layer Meteorology*, Vol. 115, pp. 1-25.

Schlatter, P., Li, Q., Brethouwer, G., Johansson, A.V., and Henningson, D.S., 2011. Structure of a turbulent boundary layer studied by DNS. ln: Kuerten H., Geurts B., Armenio V., Fröhlich J. (eds) Direct and Large-eddy Simulation Viii. ERCOFTAC Series, 15, Springer, Dordrecht, pp9-14.

Schlichting, H., 1979. Boundary layer theory, 7th edition.

Schofield, W. H., 1981. Turbulent shear flows over a step change in surface roughness. *ASME*, Vol. 103, pp. 344-351.

Shir, C. C., 1971. A numerical computation of air flow over a sudden change of surface roughness. *Journal of the Atmospheric Sciences*, Vol. 29, pp. 304-310.

Smalley, R. J., Antonia R. A., and Djenidi, L., 2001. Self-preservation of rough-wall turbulent boundary layers. *Journal of fluid Mechanics*, Vol. 20, pp. 591-602.

Taylor, P. A., 1968. On wind and shear stress profiles above a change in surface roughness. *Journal of the Royal Meteorological Society*, Vol. 95, pp. 77-91.

Wood, D. H., 1982. Internal boundary layer growth following a step change in surface roughness. *Boundary-Layer Meteorology*, Vol. 22, pp. 241-244.

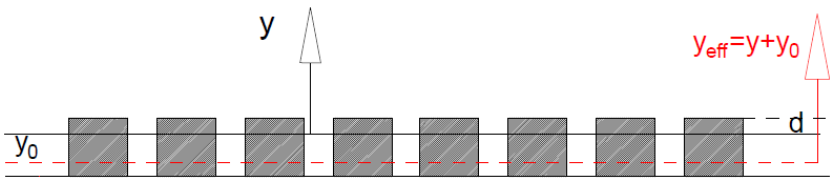

Figure 3.1. Schematic of y_{eff} and y_0 relative to the roughness elements

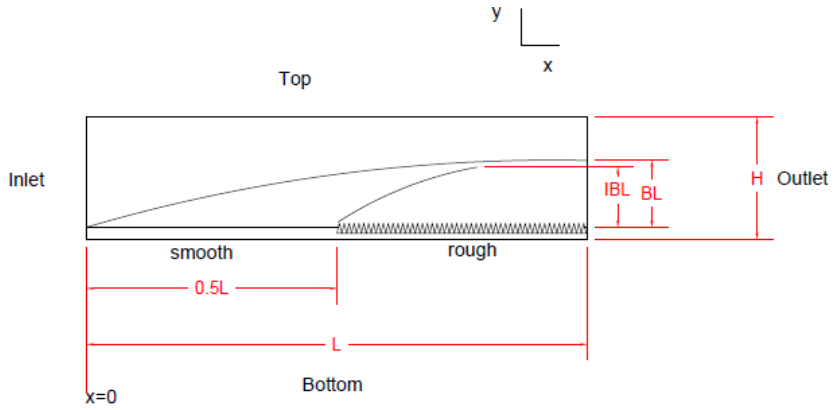

Figure 3.2. Schematic of the flow geometry

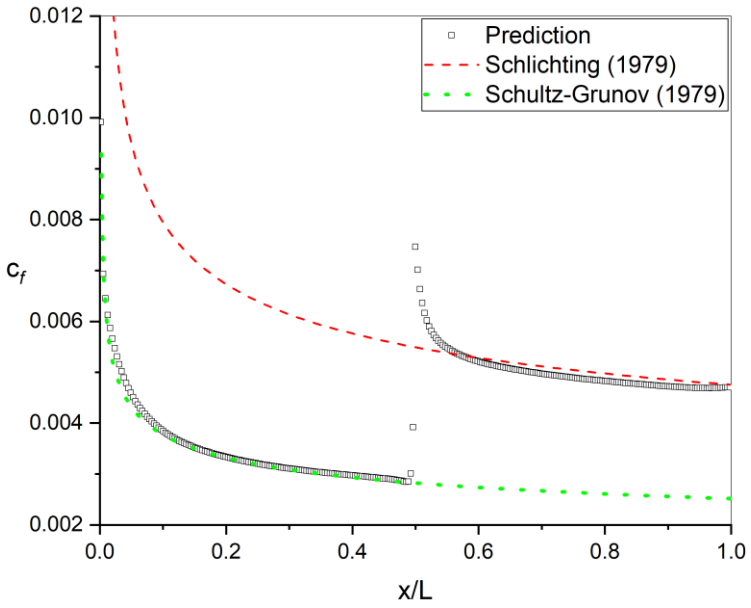

Figure 3.3. Prediction for skin friction coefficient distribution over the plate

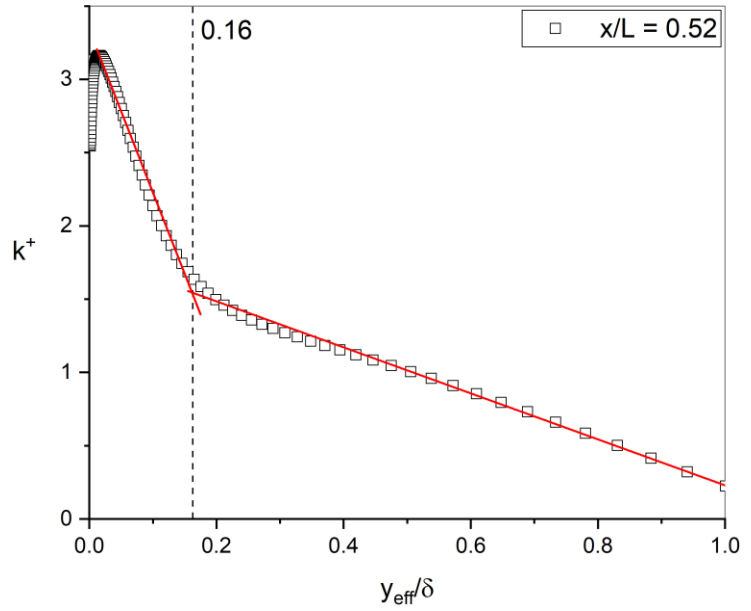

Figure 3.4. Defining the IBL thickness based on profile for the turbulence kinetic energy

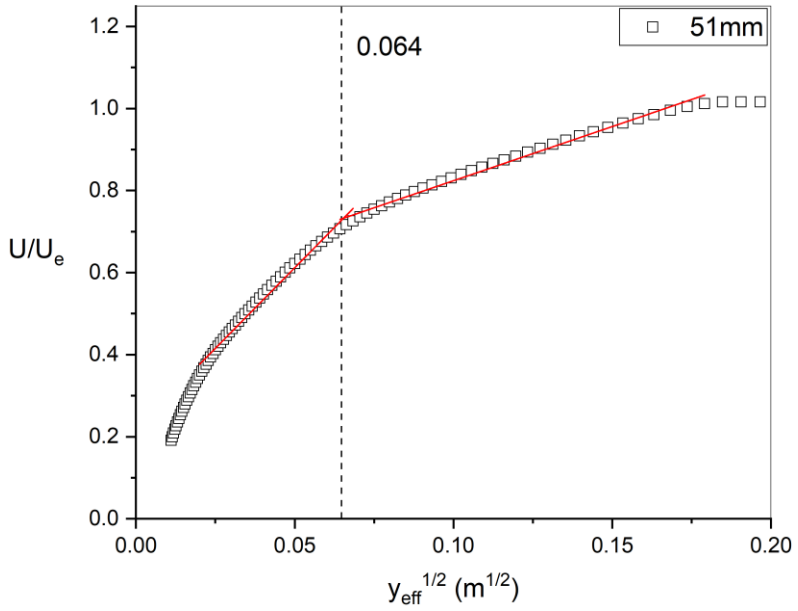

Figure 3.5. Defining the IBL thickness using the inflection point method of Antonia and Luxton (1971)

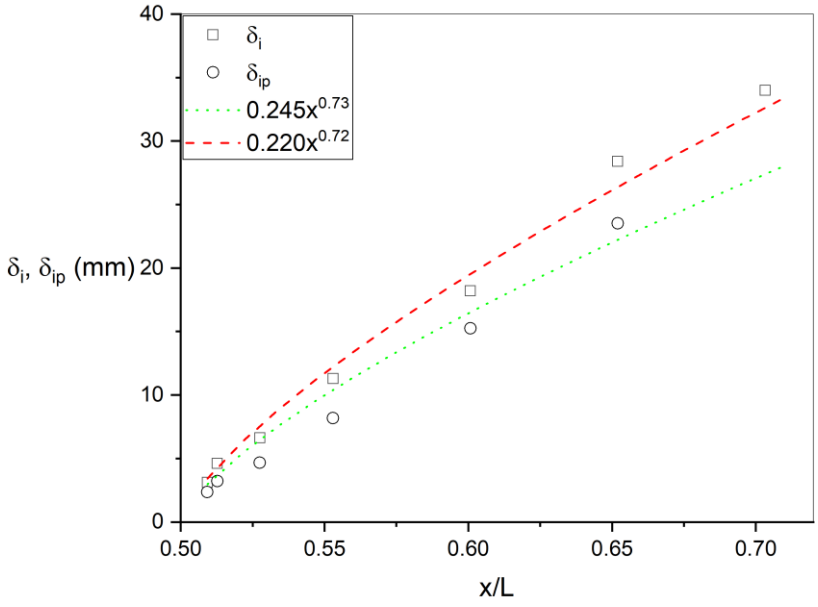

Figure 3.6. Streamwise growth of the IBL: δ_i based on the turbulence kinetic energy, and δ_{ip} based on the inflection point method of Antonia and Luxton (1971)

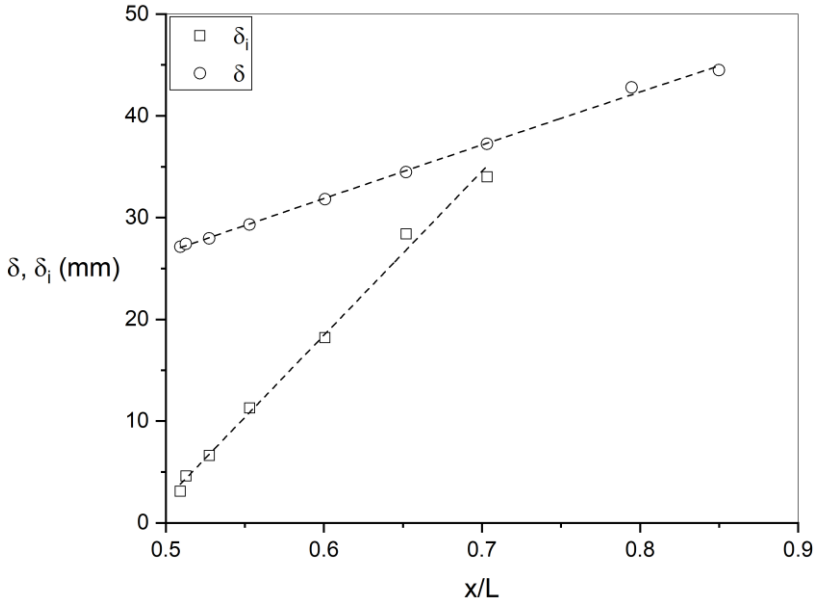

Figure 3.7. Streamwise growth of the IBL thickness compared to the outer BL thickness

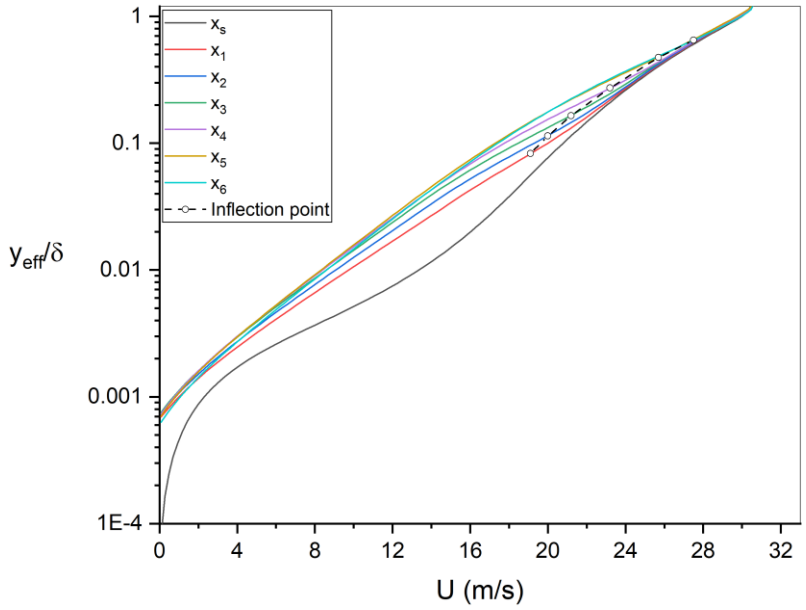

a)

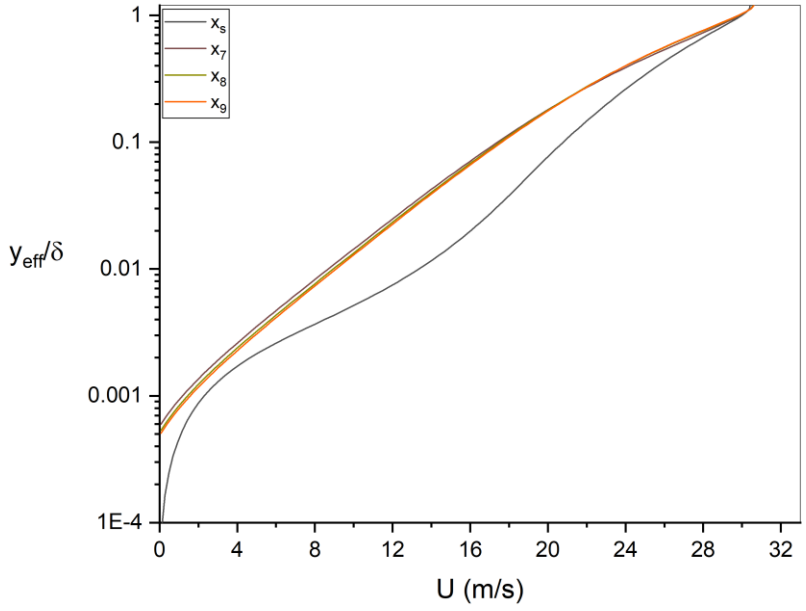

b)

Figure 3.8. a) Streamwise mean velocity profiles in the transition zone; b) Streamwise mean velocity profiles in the equilibrium zone

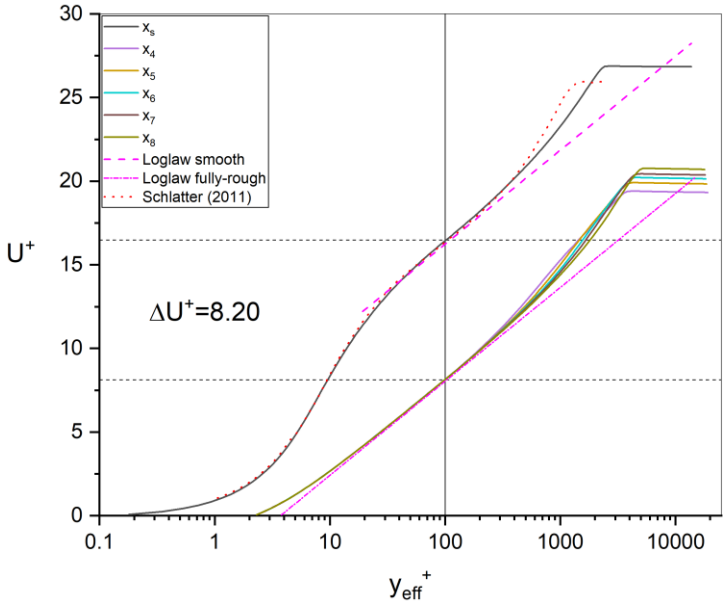

a)

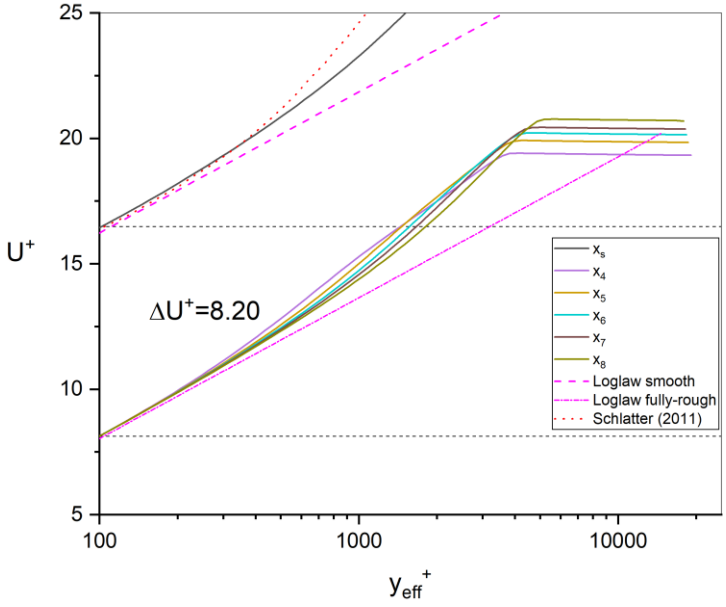

b)

Figure 3.9. a) Profile of normalized mean velocity for wall-normal direction; b) enlarged version of a) for $y_{\mathrm{eff}}^{+} > 100$

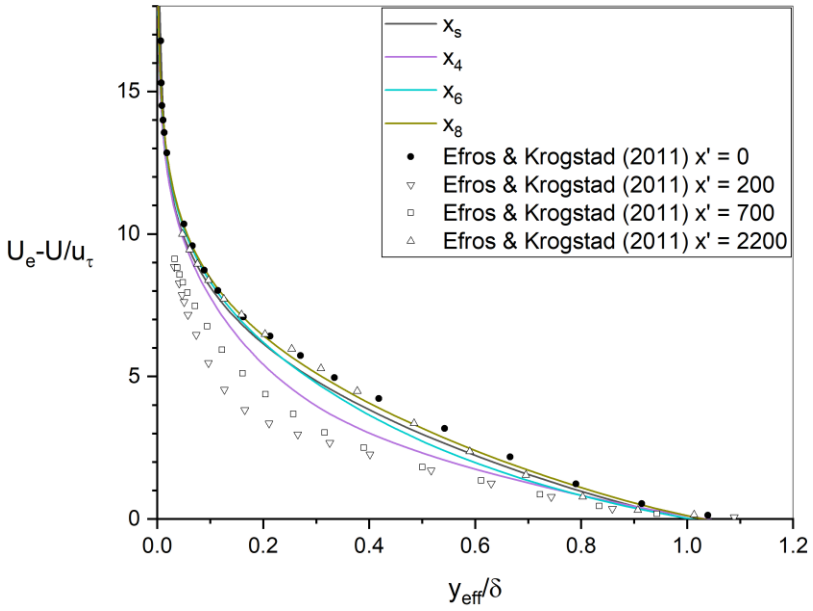

Figure 3.10. Mean velocity defect velocity profile normalized by u_τ

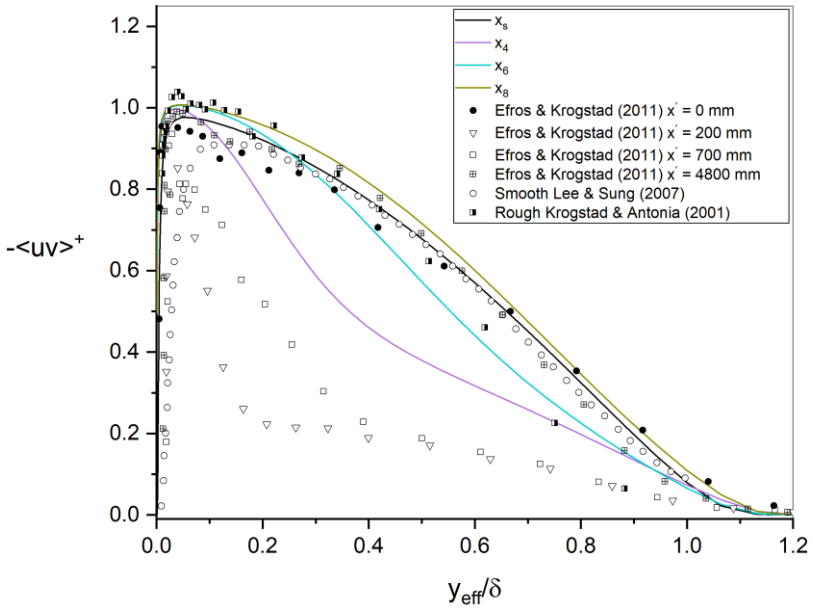

a)

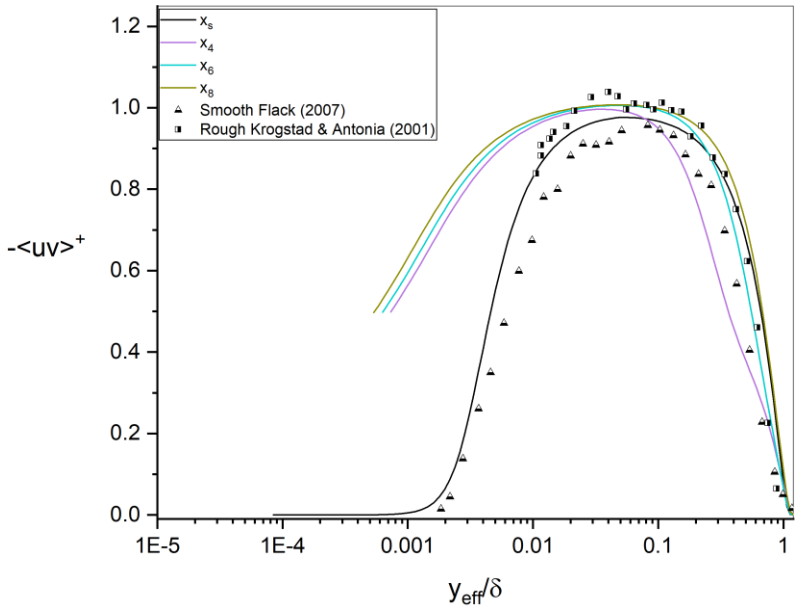

b)

Figure 3.11. a) Profile of normalized Reynolds shear stress; b) replotted using logarithmic scale for wall-normal distance

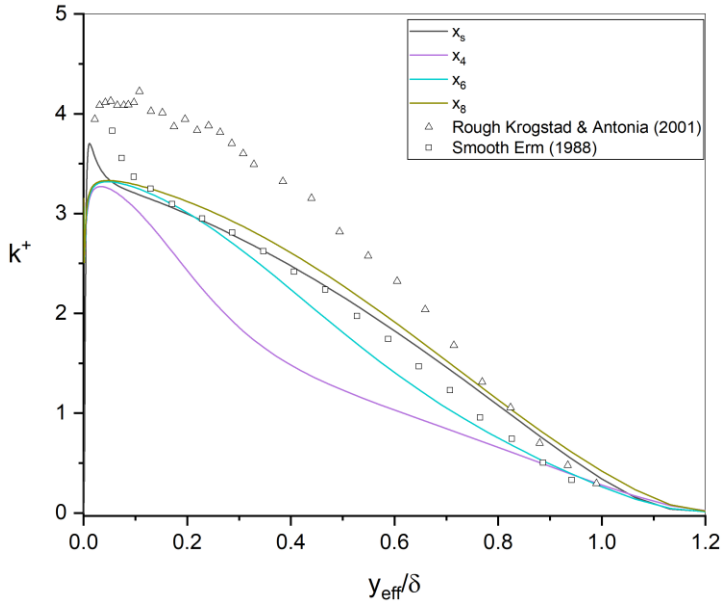

a)

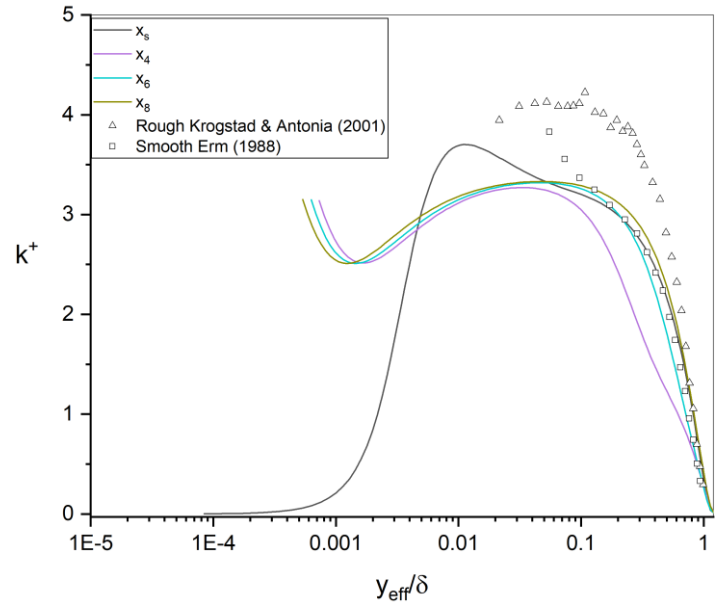

b)

Figure 3.12. a) Profile of normalized turbulence kinetic energy; b) replotted using logarithmic scale for wall-normal distance

CHAPTER FOUR

CONCLUDING REMARKS AND FUTURE WORK

4.1 Summary and Conclusion

This thesis presents a comprehensive numerical analysis of two turbulent boundary-layer flows, i.e. a vertical pipe and a flat plate, using the RANS-based two-layer $k-\varepsilon$ turbulence model of Durbin *et al.* (2001). An existing in-house 1-D code was used to perform a simulation of fully-developed pipe flow based on the two-layer $k-\varepsilon$ model for three different roughness regimes, i.e. smooth, transitionally-rough and fully rough while maintaining the same mean pressure gradient. Next, the two-layer $k-\varepsilon$ model was implemented into an in-house 2-D code, which was used to simulate the IBL created by a flow over a step change from a smooth to a fully rough surface on a flat plate. The accomplishments and findings of each study are summarized below:

4.1.1 Rough wall pipe flow

The manuscript in chapter 2 assesses the two-layer $k-\varepsilon$ model by Durbin *et al.* (2001) for the simple case of turbulent pipe flow, with special attention to the flow behavior in the proximity of the rough surface. The two-layer model correctly predicted the downward shift of the mean velocity profiles due to roughness for both the transitionally-rough and fully-rough surface conditions. Moreover, the predictions for the Darcy friction factor for the smooth and fully-rough flow cases showed a good agreement with the Colebrook (2011) correlation, however the error was relatively large for the transitionally-rough flow case.

For the same pressure gradient, the predicted eddy viscosity profiles for all three flow cases were close to each other in the outer-wall region. However, in the near-wall region the profile of the eddy viscosity for the fully-rough flow case sat significantly above the smooth and transitionally-rough flow cases. At the wall, the eddy viscosity for the fully-rough flow was finite and approximately the same as the molecular viscosity, which is consistent with the notion that the turbulence field is finite at a rough wall. The two-layer model also was able to predict the turbulence field in terms of the Reynolds shear stress and turbulence kinetic energy in the region very close to the wall. The turbulence kinetic energy exhibited two peaks in the near-wall region,

with one peak generated at the wall which was approximately the same value as the second peak typically observed in the near-wall region. For the turbulence kinetic energy budget, the two-layer model predicted zero production at the wall for the smooth-wall case and a finite value for the dissipation at the wall. The production and dissipation terms for the transitionally-rough flow case retained almost the same profile as the smooth-wall case throughout the entire boundary layer. In contrast, for the fully-rough flow case the production and dissipation profiles were changed radically due to roughness, with a dissipation rate that was much larger than finite value of production at the wall.

4.1.2 IBL created by smooth-rough transition

The manuscript in chapter 3 assesses the performance the two-layer $k-\varepsilon$ model of Durbin *et al.* (2001) for prediction of the IBL created by a flow passing over a flat plate with a step change from a smooth to a rough surface. The two-layer model was evaluated by comparison to experimental results in the literature for flows with similar features. The profile of the predicted skin friction coefficient exhibited a sharp peak at the step; for the fully developed smooth and rough regions, there was good agreement with the correlations of and Schultz-Grunov (1979) and Schlichting (1979), respectively. Downstream of the step, the mean velocity profiles exhibited the characteristic downward shift in the overlap region. The flow in the outer region was modified as the effects of the rough surface were transported into this region.

A special contribution of this paper was the use of a novel method inspired by Krogstad and Nickels (2006), based on the characteristic shape of turbulence kinetic energy profile, to determine the thickness and hence growth rate of an IBL downstream of the smooth-to-rough step change in surface roughness. The determination of the thickness of the IBL enabled two zones to be identified downstream of the step, i.e. the transition zone and the equilibrium zone. The transition zone ends and the equilibrium zone begins at the location where the outer edge of the IBL merges with the outer edge of the external boundary layer. Using the new method, the predictions for the thickness of the IBL showed a good agreement with the experimental result of Antonia and Luxton (1971). The predicted profiles for both the Reynolds shear stress and turbulence kinetic energy exhibited a peak in the near-wall region. Compared to the dimensionless smooth wall profiles, both turbulence quantities exhibited a collapse and recovery cycle in the transition region, which was indicative of the effect of the change in surface roughness. Qualitatively, this behavior was similar

to that observed in the experiment of Efros and Krogstad (2011) for a much higher roughness Reynolds number.

4.2 Future Work

The present study suggests numerous topics for future investigation that include the following:

1. For the fully-rough pipe flow, the turbulence kinetic energy exhibited a second peak at the wall, and the Reynolds shear stress was also finite at the wall. However, a wide range of experimental data is still not available for the turbulence quantities within the roughness elements, where the mean flow velocity is extrapolated to zero. Therefore, additional experiments and perhaps DNS studies could be conducted to assess both the mean and fluctuating velocity fields in the immediate vicinity of a rough wall.
2. For the smooth pipe flow, there was a discrepancy in the overlap region. This discrepancy may be reduced with the two-layer model. An analysis should be conducted to determine the reason for the discrepancy and identify methods for minimizing it.
3. There are relatively few numerical studies for the IBL based on RANS turbulence models. A wider range of RANS turbulence models, e.g the $k-\omega$ and RSM closures, should be used to analyze the mean velocity and turbulence fields after a step change in surface roughness.
4. For the IBL, there were jumps in the value of c_f immediately ahead of the step before it reached a peak value at the step. DNS and experimental studies should be performed to better understand the mechanisms for the change in skin friction in close proximity to the step.
5. For the IBL, a cycle of collapse and recovery was observed for both the Reynolds shear stress and turbulence kinetic energy. The physical mechanisms for this flow behavior should be studied more closely.
6. The two-layer $k-\varepsilon$ model was used to simulate a step configuration that might be typical of an application in engineering, with a relatively small fetch downstream of the step and using sand grain roughness. However, the ability of the two-layer model should also be tested for an environmental application with a much larger distance downstream of the step, and roughness representative of specific landscape.
7. The present study considers the case of the IBL created by the abrupt transition from a smooth to a rough surface. The rough-to-smooth and smooth-rough-smooth resembles localised

roughness and should be analyzed for the effects of roughness on the mean velocity and turbulence fields.

8. Antonia and Luxton (1999) indicated that the specific wall geometry strongly affects the turbulent transport mechanisms, especially for the near-wall region. Therefore, a comprehensive set of studies should be performed to develop a model for incorporating the effects of surface roughness in RANS turbulence models that is based on the specific geometry and distribution of the roughness elements.

APPENDIX

The standard $k-\varepsilon$ model

The $k-\varepsilon$ model focuses on the flow mechanisms that affect the turbulence kinetic energy. The instantaneous kinetic energy $\tilde{k}$ of a turbulent flow is defined as follows:

$$\tilde{k} =< k > +k \tag{A.1}$$

In equation (B1), $< k >= \frac{1}{2}(U^2 + V^2 + W^2)$ is the mean kinetic energy and $k = \frac{1}{2}(u^2 + v^2 + w^2)$ is the turbulence kinetic energy. An equation of the mean kinetic energy and the turbulence kinetic energy can be obtained by manipulating the RANS equations.

Boussinesq proposed in 1877 that the Reynolds stresses could be assumed proportional to the mean rates of deformation. The Boussinesq eddy viscosity model in Cartesian tensor notation is defined as follows:

$$-\rho < u_i u_j >= \mu_t \left(\frac{\partial U_i}{\partial x_j} + \frac{\partial U_j}{\partial x_i}\right) - \frac{2}{3}\rho k \delta_{ij} \tag{A.2}$$

In equation (A2) μ_t is the dynamic eddy viscosity. The term $\mu_t \left(\frac{\partial U_i}{\partial x_j} + \frac{\partial U_j}{\partial x_i}\right)$ is the approximation for Reynolds shear stresses, and the term $\frac{2}{3}\rho k \delta_{ij}$ is added to better account for the Reynolds normal stresses, respectively.

The standard $k-\varepsilon$ model for a Newtonian incompressible fluid in Cartesian tensor notation is defined as follows:

$$\rho \frac{Dk}{Dt} = \frac{\partial}{\partial x_j}\left[\left(\mu + \frac{\mu_t}{\sigma_k}\right)\frac{\partial k}{\partial x_j}\right] - \rho < u_i u_j > \frac{\partial U_i}{\partial x_j} - \rho\varepsilon \quad \text{(A.3)}$$

$$\rho \frac{D\varepsilon}{Dt} = \frac{\partial}{\partial x_j}\left[\left(\mu + \frac{\mu_t}{\sigma_\varepsilon}\right)\frac{\partial \varepsilon}{\partial x_j}\right] - C_{\varepsilon 1}\frac{\varepsilon}{k}\rho < u_i u_j > \frac{\partial U_i}{\partial x_j} - C_{\varepsilon 2}\rho\frac{\varepsilon^2}{k} \quad \text{(A.4)}$$

where μ is the dynamic viscosity. Typical values of the model constants that appear in equation (A3) and (A4) are as follows: $\sigma_k = 1.00$ $\sigma_\varepsilon = 1.30$, $C_{\varepsilon 1} = 1.44$ and $C_{\varepsilon 2} = 1.92$. By definition, the dynamic eddy viscosity is made proportional to a velocity scale and a length scale as follows

$$\mu_t = C\rho h l \quad \text{(A.5)}$$

where h is the velocity scale (m/s), l is the length scale (m), and C is a dimensionless constant. Since the dimensions of k and ε are m^2/s^2 and m^2/s^3, respectively, the dynamic eddy viscosity for the standard $k-\varepsilon$ model may be related to the turbulence kinetic energy, $h = k^{1/2}$, and its dissipation rate, $l = k^{3/2}/\varepsilon$, as follows:

$$\mu_t = C_\mu \rho \frac{k^2}{\varepsilon} \quad \text{(A.6)}$$

where $C_\mu = 0.09$ for the standard $k-\varepsilon$ model.

Standard wall functions

A standard wall function is a treatment for boundary conditions for the mean velocity, turbulence kinetic energy and viscous dissipation rate at high Reynolds numbers. Launder and Spalding in 1974 proposed the wall function formulation as follows

$$\frac{U_p}{u_\tau} = \frac{1}{\kappa}\ln E\left(\frac{y_p u_\tau}{\nu}\right); \qquad k_p = \frac{u_\tau^2}{\sqrt{C_\mu}}; \qquad \varepsilon_p = \frac{u_\tau^3}{\kappa y_p} \tag{A.7}$$

where U_p, y_p, k_p, and ε_p are the mean velocity, wall-normal distance, turbulence kinetic energy, and viscous dissipation rate, respectively, at the first node above the wall. E is the rough wall parameter; it has a value of $E = 9.0$ for smooth-wall flows, and can be modified to represent a rough surface.